AGU PUBLICATIONS

Geochemistry, Geophysics, Geosystems

RESEARCH ARTICLE
10.1002/2014GC005585

A comprehensive interpretative model of slow slip events on Mt. Etna's eastern flank

Mario Mattia[1], Valentina Bruno[1], Tommaso Caltabiano[1], Andrea Cannata[1], Flavio Cannavò[1], Walter D'Alessandro[2], Giuseppe Di Grazia[1], Cinzia Federico[2], Salvatore Giammanco[1], Alessandro La Spina[1], Marco Liuzzo[2], Manfredi Longo[2], Carmelo Monaco[3], Domenico Patanè[1], and Giuseppe Salerno[1]

[1]Istituto Nazionale di Geofisica e Vulcanologia, Osservatorio Etneo, Catania, Italy, [2]Istituto Nazionale di Geofisica e Vulcanologia, Sezione di Palermo, Palermo, Italy, [3]Dipartimento di Scienze Biologiche, Geologiche e Ambientali, Università degli Studi di Catania, Catania, Italy

Abstract Starting off from a review of previous literature on kinematic models of the unstable eastern flank of Mt. Etna, we propose a new model. The model is based on our analysis of a large quantity of multidisciplinary data deriving from an extensive and diverse network of INGV monitoring devices deployed along the slopes of the volcano. Our analysis had a twofold objective: first, investigating the origin of the recently observed slow-slip events on the eastern flank of Mt. Etna; and second, defining a general kinematic model for the instability of this area of the volcano. To this end, we investigated the 2008–2013 period using data collected from different geochemical, geodetic, and seismic networks, integrated with the tectonic and geologic features of the volcano and including the volcanic activity during the observation period. The complex correlations between the large quantities of multidisciplinary data have given us the opportunity to infer, as outlined in this work, that the fluids of volcanic origin and their interrelationship with aquifers, tectonic and morphological features play a dominant role in the large scale instability of the eastern flank of Mt. Etna. Furthermore, we suggest that changes in the strain distribution due to volcanic inflation/deflation cycles are closely connected to changes in shallow depth fluid circulation. Finally, we propose a general framework for both the short and long term modeling of the large flank displacements observed.

Key Points:
- Slow slip events (SSEs) have been measured at Mt. Etna
- The large amount of data observed during SSEs constrain their origin
- We infer a new model of flank sliding for the eastern flank of Mt. Etna

Supporting Information:
- Readme
- Figure S1

Correspondence to:
M. Mattia,
mattia@ingv.it (M. Mattia)

Citation:
Mattia, M., V. Bruno, T. Caltabiano, A. Cannata, F. Cannavò, W. D'Alessandro, G. Di Grazia, C. Federico, S. Giammanco, A. La Spina, M. Liuzzo, M. Longo, C. Monaco, D. Patanè, and G. Salerno (2015), A comprehensive interpretative model of slow slip events on Mt. Etna's eastern flank, *Geochem. Geophys. Geosyst.*, *16*, 635–658, doi:10.1002/2014GC005585.

Received 2 OCT 2014
Accepted 29 JAN 2015
Accepted article online 4 FEB 2015
Published online 5 MAR 2015
Corrected on 29 APR 2015

This article was corrected on 29 APR 2015. See the end of the full text for details.

1. Introduction

Ground movements at active volcanoes [see *McGuire and Saunders*, 1993 for a review] are generated by internal processes related to magma migration (inflation and deflation) or by tectonic activity (faulting, fracturing, uplift and subsidence). Diminishing mechanical strength of rocks, oversteepening and loading effects may also contribute to slope instability, failure and gravitational sliding. Fluid overpressure has been invoked as the instability mechanism for dome and flank failure [*Day*, 1996; *Voight and Elsworth*, 2000; *Reid*, 2004; *Thomas et al*., 2004]. Pressurization of fluids (mainly water and CO_2) within hydrothermal systems (regardless of eventually related magma degassing episodes) is considered the driving process of periodic deformation in restless calderas [*Dzurisin et al*., 1999; *Battaglia et al*., 2006; *Gottsmann et al*., 2007; *Hill et al*., 2002]. Structural, morphological and geophysical studies suggest that the eastern flank of Mt. Etna (eastern Sicily) is spreading seaward [see *Firth et al*., 1996 for a review]. The extent and kinematics of mobile blocks have already been widely investigated [*Lo Giudice et al*., 1982; *Lo Giudice and Rasà*, 1986, 1992;| *Kieffer*, 1983; *Guest et al*., 1984; *Borgia et al*., 1992; *Monaco et al*., 1995, 1997, 2005; *Rust and Neri*, 1996; *Gresta et al*., 1997; *Azzaro*, 1999; *Froger et al*., 2001; *Tibaldi and Groppelli*, 2002; *Lundgren et al*., 2004; *Bonforte and Puglisi*, 2006; *Solaro et al*., 2010; *Acocella et al*., 2013; *Azzaro et al*., 2013] and a complex pattern of shallow vertical-axis rotations of different blocks has also been evidenced [*Bruno et al*., 2012] but the mechanism driving flank deformation is still debated. In this paper, we discuss the origin of flank deformation at Mt. Etna by an integrated multidisciplinary analysis of ground deformations, seismicity, gas and water geochemistry data collected between 2008 and 2013. Results are employed to test a model of deformation that matches the local seismotectonic and geodynamic framework. In particular, our analysis starts from the observation of two slow slip events occurring in the eastern flank of Mt. Etna in 2009 and 2012. The existence of Slow Slip

Events (SSE) both in volcanic and seismically active areas has proved one of the most exciting discoveries in the Earth Sciences in the recent years. These events have been detected thanks to the increasing number of continuously operating GPS stations worldwide and they have been very useful toward understanding seismogenic processes in subduction zones and in identifying the transition between stable and unstable sectors beneath large volcanic edifices. So far, the only volcano where the SSEs have clearly been observed is Kilauea (Hawai'i, USA) [e.g., *Cervelli et al*., 2002; *Segall et al*., 2006; *Brooks et al*., 2006; *Montgomery-Brown et al*., 2009]. SSEs have also been observed by GPS networks worldwide in a variety of plate boundary environments [e.g., *Miyazaki et al*., 2003, 2006; *Dragert et al*., 2004; *Larson et al*., 2004]. In this work, we show that between the end of March and end of May 2009 and from March to August 2012 the CGPS network of Mt. Etna measured significant ground accelerations, particularly at the stations on its lower eastern flank. Here we propose a careful analysis of ground deformation, seismic, geochemical and geological data that show how the movements of Mt. Etna's eastern flank can be related to at least three concurrent factors: (i) the large amount of hot fluids of volcanic origin circulating beneath the eastern flank of Mt. Etna, (ii) the increasing crustal stress due to continuous rising magmatic fluids, and (iii) the circulation of water along the contact between the huge block of volcanics and the underlying Pleistocene clays. In this context, we also tried to define some basic relationships between displacements of the eastern flank and volcanic activity and to explore the possible role of fluids as a factor potentially able to contribute to the general instability of Mt. Etna's eastern flank. Finally, the geological and morphological aspects of this area provided us new and important constraints on the observed ground movements.

2. Mt. Etna's Tectonic Setting and Background Data

Mount Etna (Figure 1) is a Quaternary composite volcano, characterized by Na-alkaline magmatism, which grew to its present elevation of 3320 m by accumulation of lavas and pyroclastics, erupted during the last 200 kyr [*Gillot et al*., 1994]. It is located at the front of the Maghrebian thrust belt, on the footwall of a Late Quaternary east facing crustal scale transtensional fault system [e.g., *Monaco et al*., 1997] running in the Ionian offshore (Figure 1). The eastern and southern sectors of the volcano lie mostly on an Early-Middle Pleistocene foredeep clayey succession [*Wezel*, 1967], deposited on the flexured margin of the Pelagian block. Due to its geodynamic position, extensional tectonics has been the dominant mode of deformation controlling the time-space evolution of magmatism at Mt. Etna [*Monaco et al*., 1997, 2005; *Gresta et al*., 1997; *Azzaro*, 1999; *Patanè et al*., 2005]. Historical and instrumental seismic data show that more than 80% of earthquakes at Mt. Etna are very shallow ($h<5$ km), characterized by low energy, and located mainly on the eastern side of the volcano [*Gresta et al*., 1990, 1998; *Patanè et al*., 2004, 2005]. In this sector of the volcano shallow seismicity mostly originates from the NNW-SSE trending extensional seismogenic structures (Timpe fault system, see below). Conversely, in the western side of the volcano the distribution of earthquakes [*Gresta et al*., 1990; *Patanè and Privitera*, 2001; *Scarfì et al*., 2013] shows a clear deepening of foci on moving from the south border of the volcanic edifice toward the NNW, reaching a maximum depth of about 35 km. The analysis of fault plane solutions [e.g., *Cocina et al*., 1997; *Patanè and Privitera*, 2001; *Scarfì et al*., 2013] indicates that most events are strike-slip or oblique type, consistent with the compressive regional pattern characterizing central and western Sicily [*Palano et al*., 2012; and references therein].

The lower eastern flank of Mt. Etna is dominated by normal faulting (Figure 1). Fault segments form a 30 km long system dipping toward the Ionian Sea thatcontrol the present topography and drainage network of the eastern flank and show steep escarpments ("Timpe") with very young (mostly Late Pleistocene to Holocene) morphology. The most impressive scarps, up to 200 m high, extend discontinuously for about 20 km from Sant'Alfio to Acireale (NNW-SSE trending Timpe fault system; Figure 1). They affect sedimentary and volcanic rocks ranging in age from Early Pleistocene to historical times [A.A.V.V., 1979; *Tanguy and Kieffer*, 1993; *Corsaro et al*., 2002; *Branca et al*., 2011] and show a right-lateral component of motion [*Lo Giudice and Rasà*, 1986, 1992; *Monaco et al*., 1995, 1997; *Lanzafame et al*., 1996; *Azzaro*, 1999; *Azzaro et al*., 2013]. Most of these faults have a high seismogenic potential ($M<4.5$) and generate shallow earthquakes (<6 km) as well as coseismic cracks and creeping [*Monaco et al*., 1997; *Azzaro*, 1999, *Azzaro et al*., 2000]. Secondary structures are represented by the NW-SE striking Santa Venerina, Linera, Fiandaca and Acicatena-Valverde faults that extend upslope with poor morphologic evidence (Figure1). In the southeastern flank of the volcano, there is a less pronounced fault system, made up of two main NW-SE trending en-echelon normal-dextral seismogenic segments, the Tremestieri-Mascalucia and the Trecastagni faults.

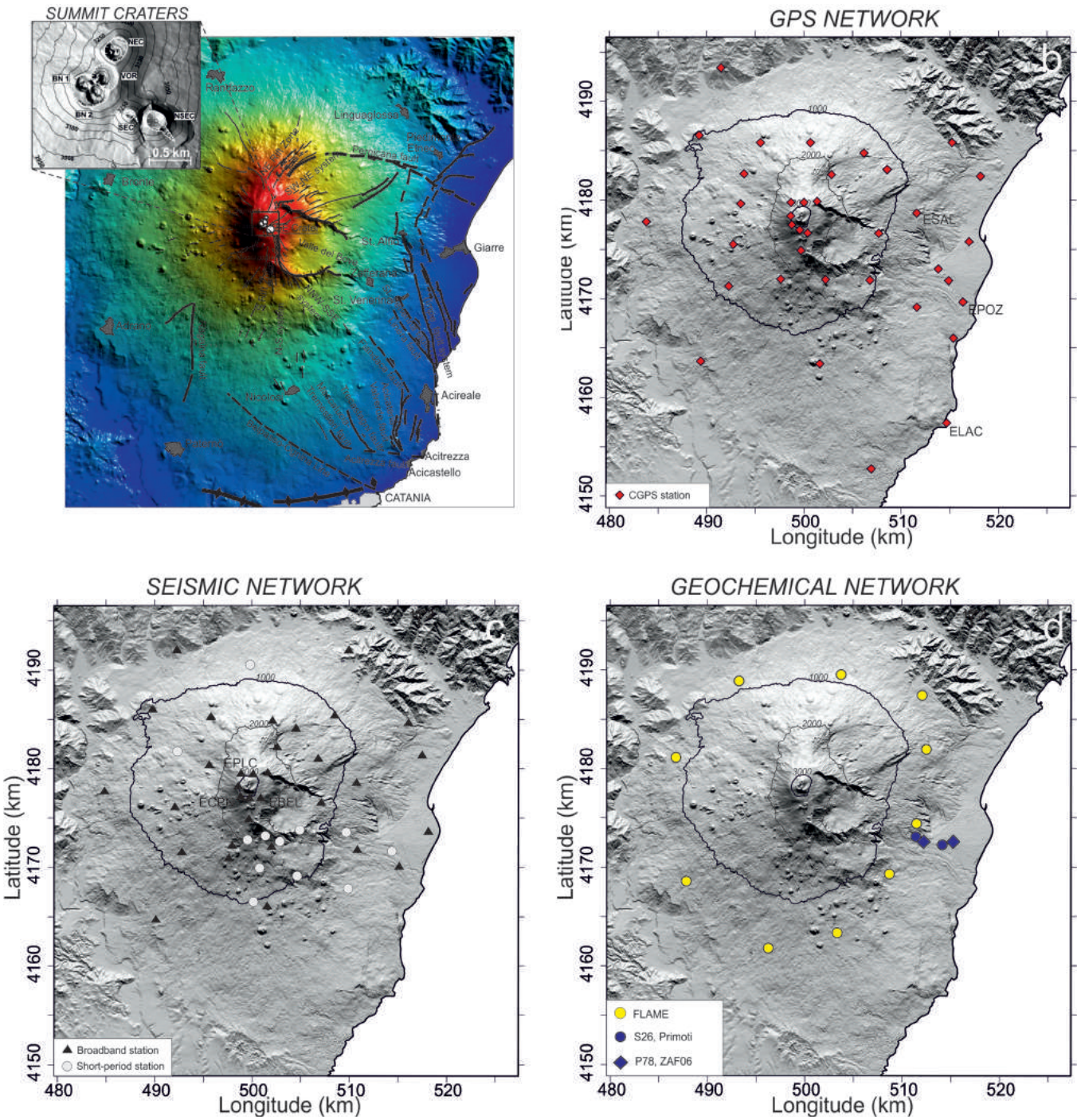

Figure 1. (a) Digital elevation model of Mount Etna volcano with the major faults and the main toponyms cited in the manuscript. Here are shown the locations of (b) GPS stations, (c) seismic stations (black triangles and gray circles for broadband and short period, respectively), and (d) geochemical stations. The inset in Figure 1a shows the distribution of the summit craters (Southeast crater, SEC; New Southeast crater, NSEC; Northeast crater, NEC; Bocca Nuova, BN1 and BN2).Colors on the main map indicate altitudes.

2.1. Aseismic Creep and Models of Flank Sliding

Aseismic creep is a common process along faults of Mt. Etna eastern flank [see *Rasà et al.*, 1996 for a complete review]. For example, creep along the eastern sector of the Pernicana fault [*Azzaro et al.*, 2001] accommodates both coseimic slip of its western sector and extension along the eruptive fissures of the NE Rift (Figure 1), whereas the Acitrezza fault accommodates coseismic slip along the Trecastagni fault (see above).

Similarly, the Acicatena-Valverde fault system is characterized by slow extensional motion that usually accomodates coseismic strike-slip deformation along the Fiandaca fault [*Monaco et al*., 2010]. Aseismic creep could also be triggered by shaking related to earthquakes along nearby seismogenic structures in a context of eastward flank sliding governed by gravity [*Rasà et al*., 1996]. Structural, morphological and ground deformation studies [see *Azzaro et al*., 2013 for a complete review] suggest that the eastern flank of Mt. Etna volcano has been sliding seaward, confirming earlier studies [*Lo Giudice et al*., 1982; *Kieffer*, 1983; *Borgia et al*., 1992; *Lo Giudice and Rasà*, 1992]. The flank deformation is characterized by complex interaction with fault systems located in the Mt. Etna eastern flank and offshore [see also *Chiocci et al*., 2011]. The sliding sector is confined to the west by the NE and S Rift zones passing through the summit craters, and to the north and to the south by the left-lateral Pernicana fault and by the right-lateral Tremestieri- Aci Trezza fault zone, respectively (Figure 1), that transfer the extensions to the east [see *Acocella et al*., 2013, and references therein]. Slope movements have been considered active for a very long time (14 ka) [*Tibaldi and Groppelli*, 2002] and with velocities of several cm/yr, but these very significant motions do not match with clear morphological, tectonic and geological evidences, especially along the southern release of the sliding area [*Branca et al*., 2014]. In particular, the Tremestieri-Aci Trezza fault zone, even though clearly evidenced by SAR and PSInSAR data [*Bonforte et al*., 2011], is only constituted by an alignment of discontinuous fractures that have been unable to define a discrete line of active dislocation [*Azzaro et al*., 2013]. According to *Firth et al*. [1996], a general process of uplifting, at rates locally exceeding 2 mm/yr, has been active since the Late Holocene along the Ionian coast of Sicily, including the coastal sector of Mt. Etna. This process is only locally interrupted by subsidence related to flank sliding of the volcanic edifice, at the hanging wall of the Timpe fault system, or is accelerated along the hinge of active anticlines (e.g., at the front of the chain in the Catania area) and at the footwall of the Timpe fault system. According to *Branca et al*. [2014], the different behavior of distinct coastal sectors can only be explained if it is assumed that the flank sliding process has only recently been superimposed on to the long-term volcano-tectonic and regional uplifting. Three main contrasting models have been proposed to explain the flank sliding: deep-seated spreading, shallow sliding and tectonic block movements [see *Firth et al*., 1996 for a complete review]. In this section, a critical examination of the proposed models of deformation is carried out.

2.1.1. Deep-Seated Spreading

According to the deep-seated spreading model [*Borgia et al*., 1992; *Rust and Neri*, 1996, *Tibaldi and Groppelli*, 2002; *Neri et al*., 2004; *Rust et al*., 2005], both the volcanic edifice and the uppermost part of its basement (down to a depth of 5 km) are spreading eastward because of magma inflation processes. Deep sliding wedges would produce a belt of active contractional structures bordering the volcano at the foot of its southern and eastern flanks. In particular, extensional deformation (1.3 cm/yr) in the summit area would be transferred to the base of the volcano through a low-angle thrust fault located at 5 km depth, deforming (0.2 cm/yr) the Quaternary foredeep sediments to the south and to the east of the volcanic edifice as fault propagation folds. However, morpho-structural studies and geomechanical considerations seem to exclude magma intrusion as the driving force of thrust faulting. In fact, the continuity of coastal emergence between the volcanic edifice and its basement [*Firth et al*., 1996; *Branca et al*., 2014], is incompatible with the differential uplift predicted by the deep-seated spreading model, which emphasizes the independent nature of Mt. Etna's mobile flank. Additionally, the occurrence of the ramp of a 5 km deep decollement, triggered by magmatic intrusion, does not find any evidence from seismic data along the Ionian offshore, where only extensional structures have been observed [*Argnani and Bonazzi*, 2005; *Argnani et al*., 2013]. As regards the on-land fold structures occurring southward they are older than the formation of the present Mt. Etna edifice and cannot be the result of deep-seated spreading [*Monaco et al*., 2002]. This system should be interpreted as a thrust-propagation fold related to the last phase of migration of the Maghrebian Chain front [*Labaume et al*., 1990; *De Guidi et al*., 2013]. Compression processes taking place at the base of the volcanic edifice are also invoked by *Borgia et al*. [1992] and *Rust and Neri* [1996] for explaining the structural setting of the pillow lavas outcropping under the Norman castle of Acicastello (Figure 1), erroneously interpreted as overturned to the south-east. Detailed field investigations of the Acicastello castle rock outcrop [*Corsaro and Cristofolini,* 2000] suggest complex emplacement conditions for both the pillows lavas and the related hydroclastic rocks that depend on pre-existing topography, lava output rate, and degree of interaction between lava, sea water and underlying unconsolidated sediments. Taken overall, these studies do not support the hypothesis of significant tilt of the whole succession that, on the contrary, appears to be little disturbed. From a mechanical point of view, models borrowed from thrust tectonics [*Davis et al*., 1993] show

that compression four to five times higher than gravitational body forces is necessary to move crustal wedges. This is incompatible with stress induced by individual dikes intruding the volcano basement.

2.1.2. Shallow Sliding

According to *Lo Giudice and Rasà* [1992] and *Rasà et al*. [1996], gravity-induced flank instability is confined by an arched tectonic structure embracing a seaward sliding sector of the volcano. This mobile sector is dismembered into minor subblocks of volcanics that slide slowly eastward under their own weight, decoupled from the sedimentary basement. Shallow sliding is also invoked by *Puglisi and Bonforte* [2004], who reconfirm the importance of detachment surfaces in the dynamics of the eastern flank of the volcano. According to these authors, the distribution patterns of the residuals between measured GPS data and modeled deformations indicate the higher mobility of the eastern and south-eastern flanks with respect to the rest of the volcano. Such enhanced mobility would be driven both by downslope movement and by the effect of volcanic sources. This model is supported by the distribution patterns of the residuals between GPS observed and modeled deformation, even though it is not backed by seismological evidences of shallow sliding planes [*Patanè et al*., 2004, 2005]. Recently, some authors [*Aloisi et al*., 2011b; *Cianetti et al*., 2012] have applied the Finite Elements Method (FEM) to verify if both shallow and deep sliding surfaces are compatible with a realistic 3-D model of Mt. Etna. Their main conclusions are summarized here:

a. *Cianetti et al*. [2012] clearly demonstrated that deeper plane is closer to the source of inflation/deflation (calculated from the inversion of ground deformation data) and it is certainly subject to a higher shear stress but also to a higher lithostatic load, while the shallower plane, being more distant from the source, undergoes a lower shear stress from the source but an equally decreased lithostatic load. As a consequence, in both cases eastward sliding takes place only along a segment of about 5–8 km from the source of inflation/deflation so that the surface deformation is fairly similar. Moreover, none of the models based on shallow or deeper sliding surfaces has been able to transfer a significant amount of horizontal deformation up the coast line where large deformations have been recorded, also associated with a negative vertical displacement, never predicted by FEM computations.

b. *Aloisi et al*. [2011b] express severe criticism of models of the eastern flank sliding and, in their opinion, the presence of medium heterogeneities may favor the eastern flank movements toward the SE and the spreading of the summit area, playing a fundamental role in ascending magma. They also investigated the shallow sliding model and found that dike forming intrusions produce negligible displacements, less than 1 mm, along the subhorizontal detachment surface. Therefore, the gravitational loading during dike forming intrusions is not able to trigger sliding processes along this plane.

2.1.3. Tectonic Block Movements

On the eastern sector of the volcanic edifice, sliding involves distinct tectonic blocks, bounded by fractures and normal and strike-slip faults, differentially. The geometry and motion of most of the major active faults and fractures are kinematically compatible between each other and thus appear to have a common tectonic origin [*Monaco et al*., 1997]. Such affinities suggest most of the extensional tectonic structures of Mt. Etna merge together at 10–15 km depth and represent shallow splays of a deep, normal fault zone driven by tectonic separation between the Ionian and the Iblean blocks, reactivated during Quaternary [*Continisio et al*., 1997; *Hirn et al*., 1997; *Nicolich et al*., 2000]. The tectonic block model is also supported by recent seismological models based on 3-D seismic tomography [*Patanè et al*., 2002, 2003, 2006]. Nevertheless, deformation rates obtained by local GPS data and SAR interferometry [*Froger et al*., 2001; *Lundgren et al*., 2003, 2004; *Bonforte and Puglisi*, 2003; *Puglisi and Bonforte*, 2004] are up to 10 times higher than those obtained by morpho-structural estimations and by permanent GPS velocity fields in other sectors of the incipient regional rift zone. This would suggest that local shallow sliding phenomena can be triggered in the eastern slope of Mt. Etna but they must be framed within the morpho-structural setting of the volcanic edifice and in the crustal seismological models, since they involve pre-existing tectonic structures at shallow levels.

2.2. Volcanic Activity Between 2008 and 2013

The time span we focused in this work starts in 2008 and ends in 2013. In this period Mt. Etna was characterized by intense volcanic activity, ranging from quiet and long-lasting effusive stages to vigorous and brief explosive paroxysmal episodes. On 13 May 2008, after a short-lived paroxysmal event on 10 May that closed a 6 month period of quiescence, a new eruptive fissure opened at the base of the South East Crater (SEC). This vent fed a lava fountaining activity which gradually evolved to a low-rate and long-lasting lava effusion

until early July 2009 [*Patanè et al*., 2013]. Four months later, a glow marked the opening of a new pit-crater at the base of SEC. Following this event the volcano remained quiescent until 2010, during which time its summit craters and the pit-crater were mostly degassing. In April 2010, explosive activity resumed consisting mainly of ash-rich explosions from both the pit and summit craters. This activity went on until January 2011 when it was gradually replaced by an intense explosive stage lasting until 2013. Over the 3 years, explosive activity consisted of 47 brief and powerful lava fountaining episodes from the New South-East Crater (originated by the afore mentioned pit crater), coupled with a copious lava flow that spread within the Valle del Bove [e.g., *Calvari et al*., 2011].

3. Data

3.1. Geodetic Data

Continuous GPS (CGPS) time series data collected between 2008 and the end of 2012 by the 38 stations of the Etn@net network have been processed using the GAMIT/GLOBK software packages [*King and Bock*, 2004; *Herring*, 2004] and applying the method described in *Bruno et al*. [2012] and *Aloisi et al*. [2011a]. The East component of the daily GPS position time series at the ELAC (Lachea Island, see Figure 1) site in Figure 2 shows a sequence of five significant offsets occurring on 14 April 2009, 24 May 2009, 15 April 2010, 17 March 2012 and 24 June 2012, interpreted as accelerated eastward displacements. These events lasted 1 or 2 days, had maximum displacements up to 2 cm and were not correlated to any particular volcanic event in this period. Instrumental effects were also excluded since the amplitude of these events were beyond any standard noise induced by sources that are usually considered to affect CGPS time series [*Mao et al*., 1999]. Similarly, they were not observed in the time series of distant CGPS stations from the eastern flank, thus ruling out the possibility that displacements were artifacts of unmodeled errors in GPS time series. Moreover, these events were not related to concurrent earthquakes occurring on the volcano or elsewhere and any possible instability of the pillar on which the GPS antenna is mounted has been excluded. On 31 March 2010 an offset occurred in the East component of the position time series of site ESAL in the Eastern flank. This offset preceded by some days the 2010 offset of ELAC and was accompanied by a sequence of trending changes observed on 31 March 2009, 24 May 2011, 18 July 2011, 13 March 2012 and 12 August 2012. Similar trending changes were observed also in the EPOZ time series on 09 April 2009, 23 August 2012 and 23 May 2013. By analyzing the temporal evolution of these displacements we can observe some features: 1) Evidence of propagation of deformation in the eastern flank of the volcano as testified by the different starting of the increased velocity at the different stations; 2) The time series show that there are different modalities of strain release at the different CGPS stations. In particular, the ELAC station time series show a brittle behavior (sudden changes), when compared to those of the other two stations (gentle slope change); 3) Considering the duration of the increased velocity of the eastern flank both in 2009 and in 2012, we can say that their duration is comparable (about 2 months). In Figure S1 (supporting information) the velocities of the Mt. Etna CGPS network for the two slow slip events are also shown.

These observations, coupled with the lack of seismic activity directly related to the early phases of the event and/or located in the area showing the largest displacements, point to considering these processes in the class of "silent" earthquakes or slow slip events (SSE) in a volcanic environment, defined for the first time by *Cervelli et al*. [2002] for the south flank of Kilauea volcano.

3.2. Seismic Data

The Mt. Etna permanent seismic network, managed by Istituto Nazionale di Geofisica e Vulcanologia (INGV)-Osservatorio Etneo, comprises 32 broadband and 12 short-period stations (Figure 1c).

Volcano-tectonic (VT) earthquakes, occurring at Mt. Etna during 1 June 2008 to 30 June 2013 (*Gruppo Analisi Dati Sismici*, 2015), were studied and the following information obtained: map of Mt. Etna with the locations of all the VT earthquakes taking place during the period of interest (Figure 3); seismic strain release maps of VT earthquakes with depth $>$ 10 km b.s.l. occurring during 4 month periods (Figure 4); daily number of VT earthquakes, located in the dashed area in Figure 4 with depth $>$ 10 km b.s.l., and corresponding cumulative seismic strain release curve (Figure 5). As shown by Figure 3, the distribution in the map of the VTs reflects the distribution in depth. Indeed, in the eastern flank and beneath the summit area very shallow earthquakes (red and orange dots; depth $<\sim$7 km) are concentrated. In particular, the shallowest ones took place in the north-eastern flank, along the Pernicana fault system. In the southern flank earthquakes

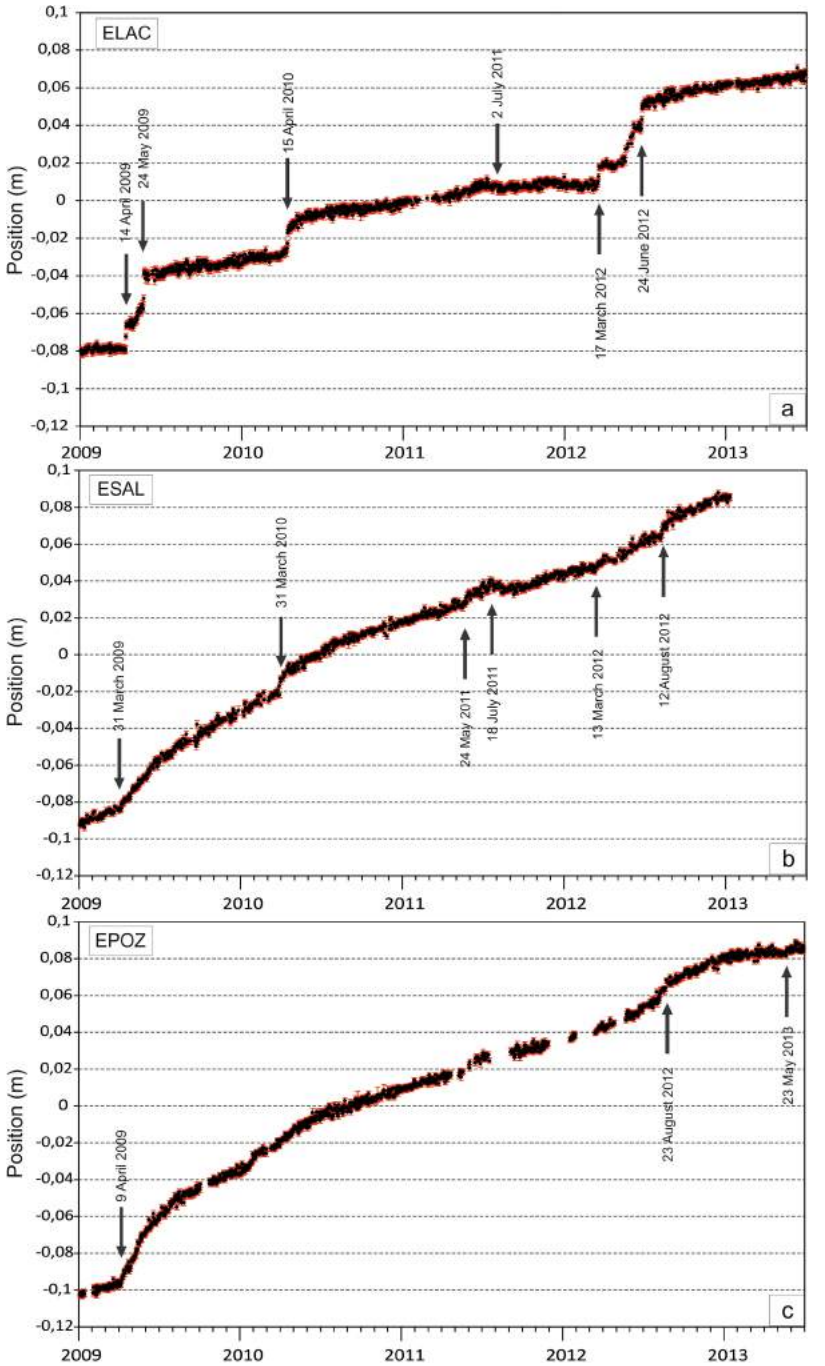

Figure 2. East component of the daily GPS position time series for the ELAC, ESAL and EOPZ GPS stations. Red error bars show the 95% confidence intervals. Black arrows indicate the most significant offsets or trend changes together with the date of the corresponding event.

characterized by intermediate depth (yellow dots; depth ranging from ∼10 to 17 km) are clustered. Finally, in the north-western flank the deeper seismicity (blue dots; depth > ∼20 km) took place. During the entire analyzed period significant VT activity was concentrated in the north-eastern flank along the Pernicana fault system, culminating in important sequences taking place in August 2009, April 2010, and August 2012 (Figure 4). Focusing on the eastern and south-eastern flank of the volcano, characterized by the Timpe fault system, significant VT increases occurred in March–July 2009 and June 2012 to March 2013, as testified by both strain release maps and VT cumulative strain release curve (Figures 4 and 5). In both the aforementioned cases the VT earthquakes were spread out over the eastern and south-eastern flanks.

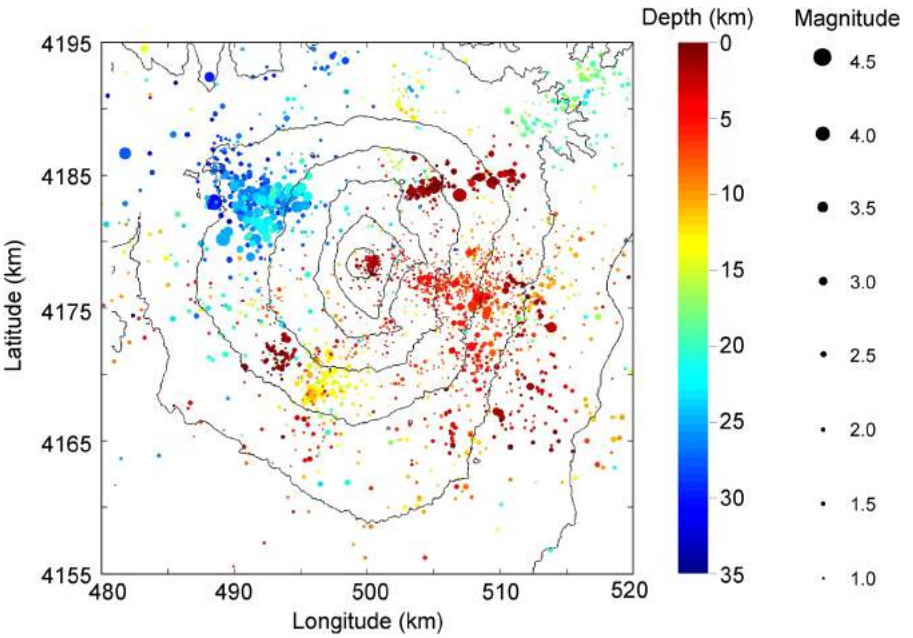

Figure 3. Map of Mt. Etna with the location of the VT earthquakes taking place during the period 1 June 2008 to 30 June 2013. The size and color of the dots indicate the magnitude and the depth of the VT earthquakes, respectively (see legend).

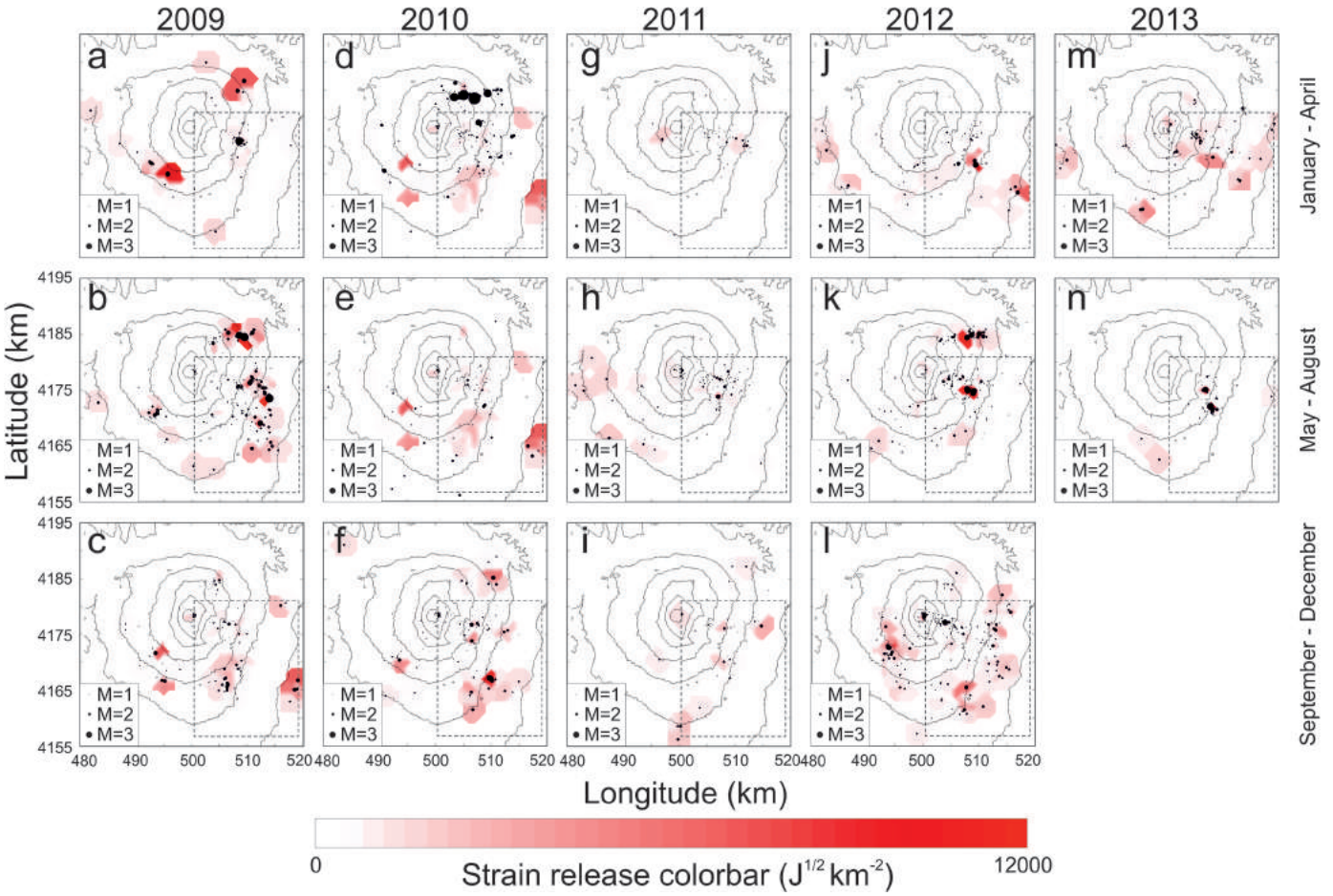

Figure 4. Seismic strain release maps of VT earthquakes with depth > 10 km b.s.l. occurring during 4 month periods. The black dots indicate the location of the VT earthquakes. The dashed rectangles in the volcano eastern flank show the area whose seismicity is analyzed in Figure 5.

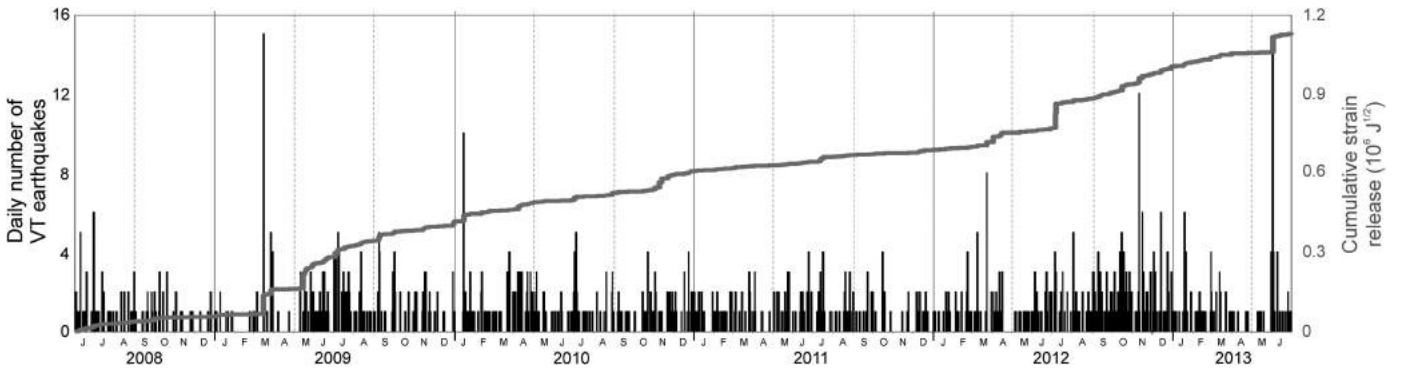

Figure 5. Daily number of VT earthquakes located in the dashed area in the maps of Figure 4 with depth > 10 km b.s.l. (histogram), and corresponding cumulative seismic strain release curve (gray line).

To study the behavior of volcanic tremor and long period (LP) events during the period of interest, the following information was obtained (Figure 6): i) seismic RMS; ii) volcanic tremor source locations and; iii) daily number and amplitude of LP events. RMS of the seismic signals, recorded at the vertical component of ECPN and EPLC stations (see Figure 1), was obtained as daily median values calculated over RMS of 10 s-long sliding windows (Figure 6a). The tremor source locations were retrieved by following the approach described by *Di Grazia et al*. [2006] and *Cannata et al*. [2013], inverting the spatial distribution of tremor amplitude in 8–19 stations using a grid-search approach (Figures 6b–6d). Concerning LP events, ECPN station was used as a reference station because of its longest record (Figure 1), with the exception of the period January–March 2009 when EBEL station was used as reference because of the lack of ECPN data. Regarding volcanic tremor locations, three main changes can be noted: April–May 2009, November 2010 and April–May 2012. During the first period (up to April–May 2009), roughly coinciding with the 2008–2009 eruption, the tremor source centroids were located below the eruptive fissure, that opened east of the central craters. In April–May 2009, tremor sources shifted north-westward. Such change was temporary, as shown by the gradual shift of the tremor again toward the 2008–2009 eruptive fissure. During November 2010 the tremor source sharply shifted toward NEC and deepened (from ∼2.5 a.s.l. to ∼1.5 a.s.l.). Finally, in April–May 2012 the tremor source centroids shifted again south-eastward and became shallower (up to 2.0–2.5 km a.s.l.). The periods, characterized by the most energetic LP events, were April–June 2009 and February–June 2013 (Figure 6f). While the latter period coincides with the first lava fountain cycle in 2013, the former, more important than the latter in terms of LP amplitudes, was accompanied by no visible changes in the volcanic activity.

3.2.1. Seismic Tomography of Mt. Etna

Mt. Etna's tomographic models contribute significantly to clarify whether and how tectonic control of magma ascent works at Mt. Etna, revealing a broad complex of intrusive meshes in the upper and middle crust. In particular, here we reanalyze the results obtained by the last tomographic study performed by *Patanè et al*. [2006] and *Alparone et al.* [2012]. In summary, the main features revealed by Mt. Etna Vp tomography [*Patanè et al*., 2006, Figure 7] are:

1. A shallow high Vp anomaly (Vp ranging between 3.5 and 5.5 km/s) beneath the southern craters, the South Rift and mostly beneath the central-southern sector of the Valle del Bove, between 0 and −1 km depth, is interpreted as a solidified intrusive complex (Figure 7a). Contours for 3.5–5.0 km/s at 0 km show that the high velocity anomaly aligns with the present-day south and northeastern Rifts. The presence of the old shallow plumbing system feeding the past Mt. Etna eruptive centers (e.g., Trifoglietto volcano), located along the central-southern part of the Valle del Bove, is also evidenced both at 0 and −1 km a.s.l.. These higher velocity volumes can be linked to: (i) the wide plutonic body mainly located beneath the Valle del Bove [*Patanè et al*., 2003, 2006]; (ii) the solidified magma reservoirs feeding the S, NE and ENE Rift zones.

2. A high Vp body (Vp ranging between 5.5 and 6.7 km/s), trending NNW-SSE to NS located beneath the central craters and extending toward S and SSE, between −2 and −15 km a.s.l. (wide 5–7 km in longitude and 8–10 km in latitude) is interpreted as high density cumulates, fractionated by the magma during its ascent, stocked and congealed at depth (Figures 7 a and 7b).

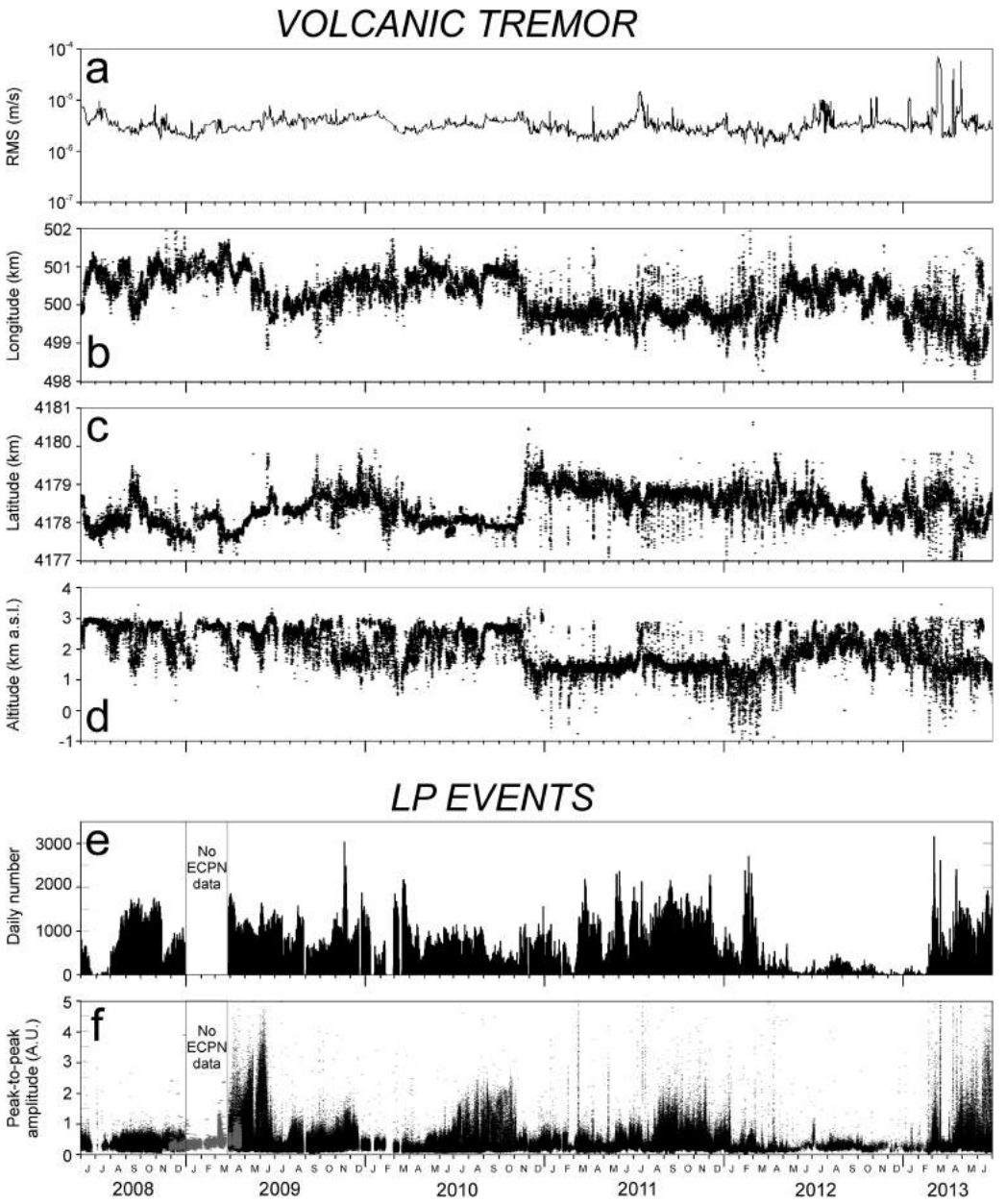

Figure 6. (a) RMS of the vertical component of the seismic signal recorded at ECPN and EPLC stations, obtained as daily median values calculated over RMS of 10 s-long sliding windows. (b) Longitude, (c) latitude, and (d) altitude of the volcanic tremor source centroids, calculated within 1 h-long windows. (e) Daily number of LP events. (f) Peak to peak amplitude of the LP events calculated at ECPN (black dots) and EBEL (gray dots) stations.

Therefore the high Vp intrusion is the main structural feature of the volcano, testifying to its intense past history, and revealing the accumulation of a very large volume of nonerupted volcanic material. The bulk of the high Vp body, located to the southeast of the central craters, suggests that the Valle del Bove has been the main site for magma accumulation in the past as confirmed by the presence of the old eruptive centers (e.g., Trifoglietto). The high Vp body, trending NNW-SSE to NS between −1 and −5 km depth appears rooted at slightly greater depth. At present, the ascent of magma is controlled by the pervasive high Vp intrusion and occurs at its western border (beneath the southern Rift). Very shallow dike emplacement at the border of the intrusive body occurs mostly on NNW trending fracture system (S Rift), such as those of the 2001 and 2002–2003 eruptions, and along the NE Rift. The structural features and seismicity of Mt. Etna is rather complex. In the last three decades, seismicity mainly occurred at the borders of the high Vp body

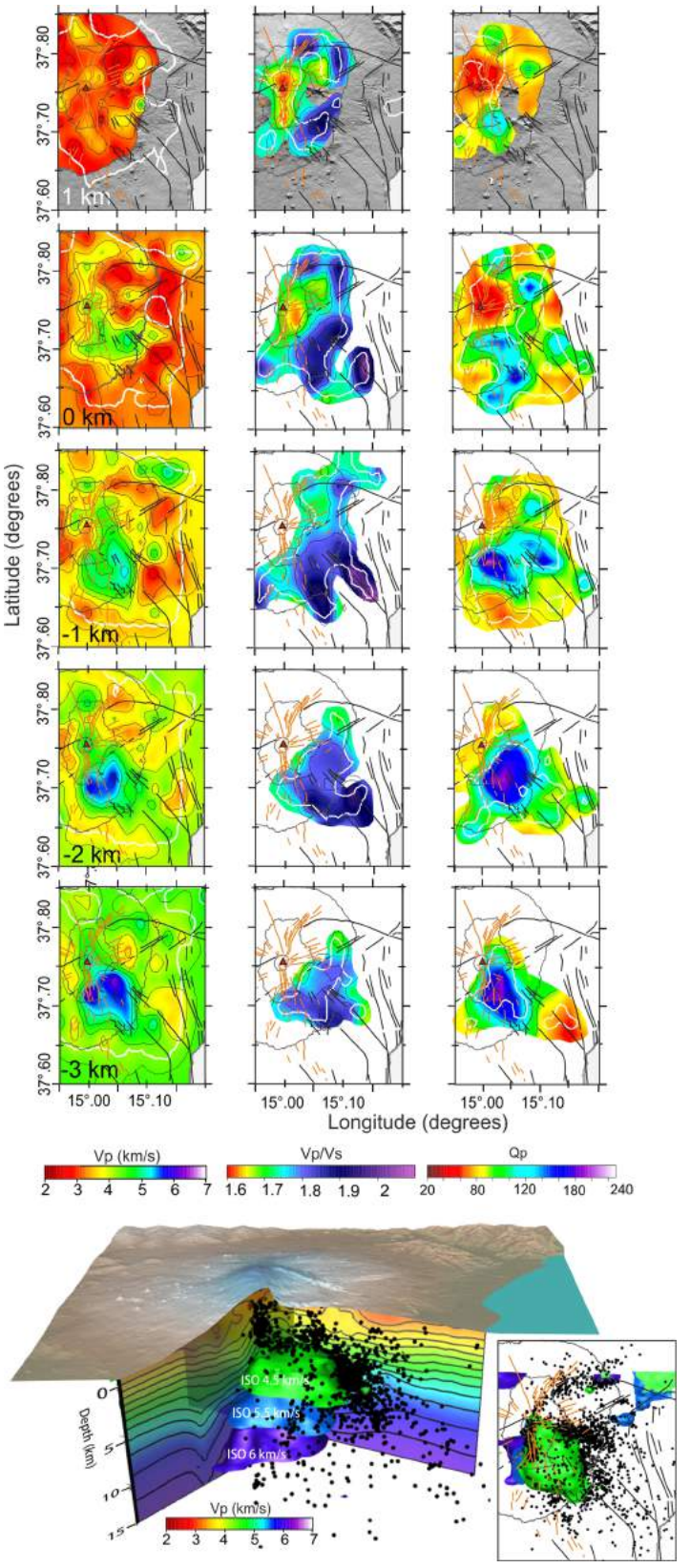

Figure 7. Tomographic image of Mt. Etna (modified from data previously published by *Patanè et al.* [2006] and *Alparone et al.* [2012]). (a–e) Different slices at different depths. The final 3-D model shows both the isosurfaces of three different levels of Vp velocities and the distribution of seismicity.

that appears almost like an aseismic volume (Figure 7b). On the shallow layers of the volcano, seismicity affects several clearly recognizable fault and fissure systems (Figures 7a and 7b).

Considering the two main clusters of seismicity in the central-northeastern sector, these delineate the margins of a fairly shallow aseismic depression WNW-ESE elongated. In Figure 7b, the tomographic isosurfaces show the geometry of the high Vp volume. It is evident that the WNW-ESE elongated seismic cluster, is affecting the northern border of the high Vp volume at several depths. The Pernicana fault system, showing continuity with the NE Rift, can be related to a transition region between the lower velocity deposits of the depression and the discontinuous high velocity zones recognizable in the north (Figure 7a). It is noteworthy that the distribution of seismicity in the eastern and southern flanks occurs along several and shallow fault segments, allowing possible tectonic block movements. Then a large-scale sliding of the eastern flank of Etna and the existence of a unique decollement plane (deep or shallow) is not supported by seismic observations.

A similar scenario is the East-Rift zone of the Kilauea volcano, where a decollement plane has been well recognized and strong earthquakes occur on quasi horizontal reverse fault planes [e.g., *Wolfe et al.*, 2003].

3.3. Geochemistry of Fluids

3.3.1. Plume Chemistry and Soil CO_2 Degassing

Mt. Etna bulk SO_2 flux was measured by means of the FLAME (FLux Automatic MEasurement) scanning ultraviolet spectrometer network [*Salerno et al*., 2009a, 2009b; *Campion et al*., 2010; *Merucci et al*., 2011]. This consists of ten stations spaced ~7 km apart and installed at altitudes of ~900 m a.s.l. on the volcano flanks. The halogen fluxes were calculated combining the SO_2 flux with the SO_2/HCl and SO_2/HF weight ratios determined by ground-based Fourier Transform Infra-Red (FTIR) spectrometry [*La Spina et al*., 2010]. Measurements were carried out periodically (about three times per week) from distal sites located about 14 km from Mt. Etna summit area, depending on the position of the sun and wind direction. Periodic measurements of soil CO_2 efflux (expressed in g m^{-2} d^{-1}) were carried out at a site named ZAF06, located on the east flank of the volcano at an altitude of about 500 m a.s.l. (Figure 1), using the method of the dynamic accumulation chamber [e.g., *Parkinson*, 1981; *Chiodini et al*., 1998]. The site chosen is located on a WNW-ESE directed fault system that is known as an important degassing zone [*Giammanco et al*., 1995; *Giammanco and Bonfanti*, 2009]. This site is characterized by particularly high soil CO_2 efflux and by a representative temporal pattern of CO_2 emission [e.g., *Giammanco et al*., 1995; *Giammanco and Bonfanti*, 2009]. Gases from this site are assumed to derive from a relatively shallow portion (~5 – 10 km) of the magma feeder system of Mt. Etna [*Giammanco et al*., 1998; *Bruno et al*., 2001]. Measurements were carried out approximately once per month and data cover the period from 1 January 2009 to 30 June 2013. Continuous CO_2 flux measurements were made with the dynamic (or dilution Cd) method [*Gurrieri and Valenza*, 1988] at a site known as P78. This site is located some 3 km east of site ZAF06 along the same structural lines, and it is characterized by higher emissions of CO_2 associated with other magmatic gases [*Giammanco et al*., 1995; *Giammanco et al*., 1998; *Giammanco and Bonfanti*, 2009]. The monitoring station is part of the EtnaGAS network and monitored parameters are: CO_2 soil flux and atmospheric parameter (T, P, Rh, rain, wind speed and wind direction; *Liuzzo et al*. [2013] and *Gurrieri et al*., [2008]. Data were collected with hourly frequency. Figure 8b shows the 14 days moving average of SO_2 and halogen fluxes in the plume, as well as the values of soil CO_2 efflux from site ZAF06 and the daily averages of soil CO_2 flux continuously recorded from site P78 between January 2009 and 30 June 2013. Over the 60 month period of observation daily SO_2 emission rate was characterized by a mean emission rate of ~2500 Mg d^{-1} (standard deviation $1\sigma = 800$ Mg d^{-1}). Halogen fluxes (HCl and HF) showed average values, respectively, of 454 Mg d^{-1} (standard deviation $1\sigma = 287$ Mg d^{-1}) and of 86 Mg d^{-1} (standard deviation $1\sigma = 79$ Mg d^{-1}). Soil CO_2 efflux values at site ZAF06 showed an average of ~810 g m^{-2} d^{-1} (standard deviation $1\sigma = 1200$ g m^{-2} d^{-1}), with peaks up to about 6700 g m^{-2} d^{-1}, that is to say the highest average and peak values since the beginning of observations at this site in 2006 (S. Giammanco, personal communication, 2014). Lastly, soil CO_2 flux values at site P78 showed an average of ~ 793.13 g m^{-2} d^{-1}(standard deviation $1\sigma = 560.72$ g m^{-2} d^{-1}). Overall, volcanic degassing from Mt. Etna during the study period shows three different stages. The first stage relates to the period between the final months of the long-standing 2008–2009 eruption and late 2009. During this period both bulk plume and diffuse degassing were low. This behavior changed from April to May 2009 when diffuse CO_2 emissions started to increase significantly at both monitored sites (ZAF06 and P78), with spike-like variations at ZAF06 and a more uniform trend at P78. Anomalies were followed by an increasing trend in crater SO_2 flux, mostly evident in October–December 2009, but not by an appreciable increase in halogen fluxes.

A second stage of anomalies started in September 2010, matched by an increase in SO_2 flux after having fallen to low levels. Unlike the second half of 2009, during this period also crater halogens emissions increased markedly and concurrently with SO_2 fluxes and CO_2 emissions. Diffuse CO_2 emissions increased again after some weeks of seemingly lower values. In early 2011, together with the onset of the sequence of lava fountaining episodes from the pit-crater of SEC, soil CO_2 emissions gradually decreased until reaching very low background values in early 2012. Crater SO_2 fluxes, during this stage, showed a rather fluctuating behavior, with several cycles of emission lasting some weeks to some months, and a general trend toward decreasing values until the 2012 summer. A similar pattern was observed for the halogen fluxes, although their values were much higher than in the previous stage and reached some of the highest levels ever. Subsequently, as for diffuse CO_2 emissions, halogens also showed a period of relatively low values, from late 2011 to about April 2012.

The third and final stage in volcanic degassing was observed from March to April 2012, when diffuse CO_2 emissions increased again, this behavior being mostly visible at site P78. Crater SO_2 fluxes continued to show a fluctuating pattern with relatively high average values, but without any clear trend, whereas

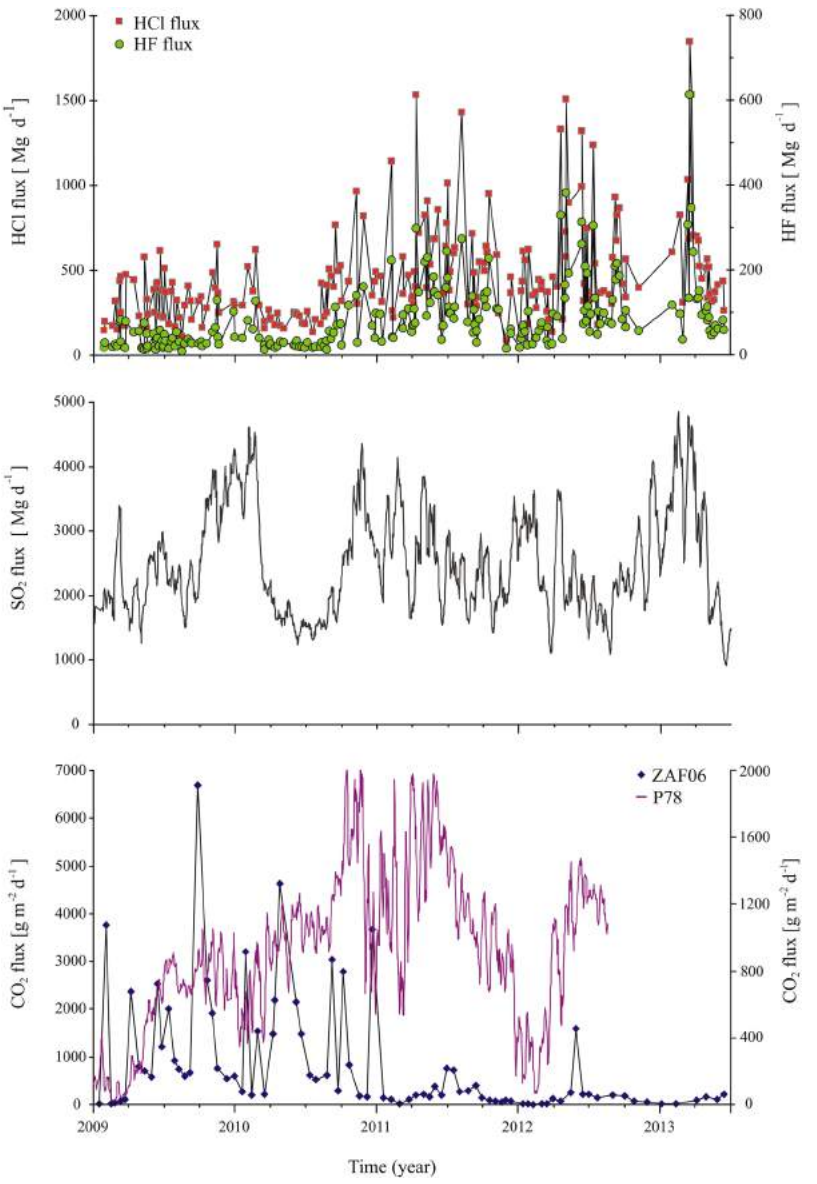

Figure 8. From bottom to top, CO_2, SO_2, HCl and HF flux in the period between January 2009 and June 2013.

halogen fluxes had a renewed and strong increase in their values that lasted more or less until the end of the study period. The temporal patterns described above for crater and diffuse degassing can be interpreted according to the dynamics of magma ascent and degassing in the feeder system of Mt. Etna. As expected by their solubility versus depth behavior upon ascent [e.g., *Pan et al*., 1991; *Carroll and Holloway*, 1994], anomalous emissions of CO_2 from a volcano mark early stages of fresh magma degassing at depth, whereas anomalous emissions of SO_2 and halogens mark the arrival of new batches of magma at shallow levels within the volcano feeder system. The low values of SO_2, HCl and HF emission rates in early 2009 suggest that the magma body that had supplied the 2008–2009 eruption was almost exhausted in volatiles. Replenishment of the shallow feeder system of Mt. Etna with new gas-rich magma, arriving from depth $>$5 km beneath the volcano surface, probably occurred in each of the four stages described above, as evidenced by the very high CO_2 emissions recorded. The shallow ($<$4 km below the surface) dynamics of magma in the main volcanic conduits (e.g., a pulsating mechanism of magma migration toward the surface) is probably responsible for the observed fluctuations of SO_2 and halogen fluxes during 2011 and 2012.

3.3.2. Groundwater Chemistry

Water temperature, electrical conductivity (EC), and phreatic level, as well as total dissolved gas pressure (TDGP) and CO_2 partial pressure were acquired with hourly frequency by two geochemical monitoring stations operating on the eastern flank of Mt. Etna, belonging to "ETNAACQUE" network. The monitoring stations host sensors for temperature (NTC 10K range: 0–100°C ± 0.1°C), EC (customized 4 electrodes sensor AISI316 range 0–4000 μS ± 10 μS), TDGP (customized pressure sensor MPX2100 AP PTFE membrane interfaced) [*De Gregorio et al*., 2005]. Figure 9 shows the time record of temperature and EC measured in s26, along with data on temperature, EC and TDGP measured in the Primoti well during the study period. As concerns the drainage gallery s26, an almost continuous trend of decreasing water temperature and salinity (here represented by the EC), is observed until the end of 2008. From 2009 onward, while water temperature still decreases, the water salinity (i.e., EC) starts an increasing trend, which reversed in the first months of 2011. From mid-2012 onward, EC shows again an increasing trend, still ongoing at the end of the observation period. Primoti well data are available from October 2009. Water salinity was constantly higher than that measured in the drainage gallery s26, yet its values in general showed a similar behavior as those measured in s26. The higher salinity recorded at Primoti is due to higher CO_2 dissolution and hydrolysis, which enhances rock leaching and ion release in water solution [*Brusca et al*., 2001]. In detail, water temperature, water salinity and TDGP recorded at Primoti well show intra-annual variability. In particular, from April to July of each year (shaded areas in Figure 9), both water temperature and water salinity declined, while TDGP increased concurrently. Both s26 and Primoti sites are fed by the same catchment and hence have similar temperature and chemical composition (INGV database, unpublished data, 2014). However, the most striking difference between them concerns the saline content of water, which is higher in Primoti well (Figure 9c). The significant changes in salinity (through EC values, plot in Figure 9c), observed at s26 over the whole study period, associated with changes in and the relative concentration of dissolved ions (INGV database, unpublished data, 2014), suggest that this gallery drains water that results from mixing of at least two end-members with different saline content whose respective contribution changes over time. In

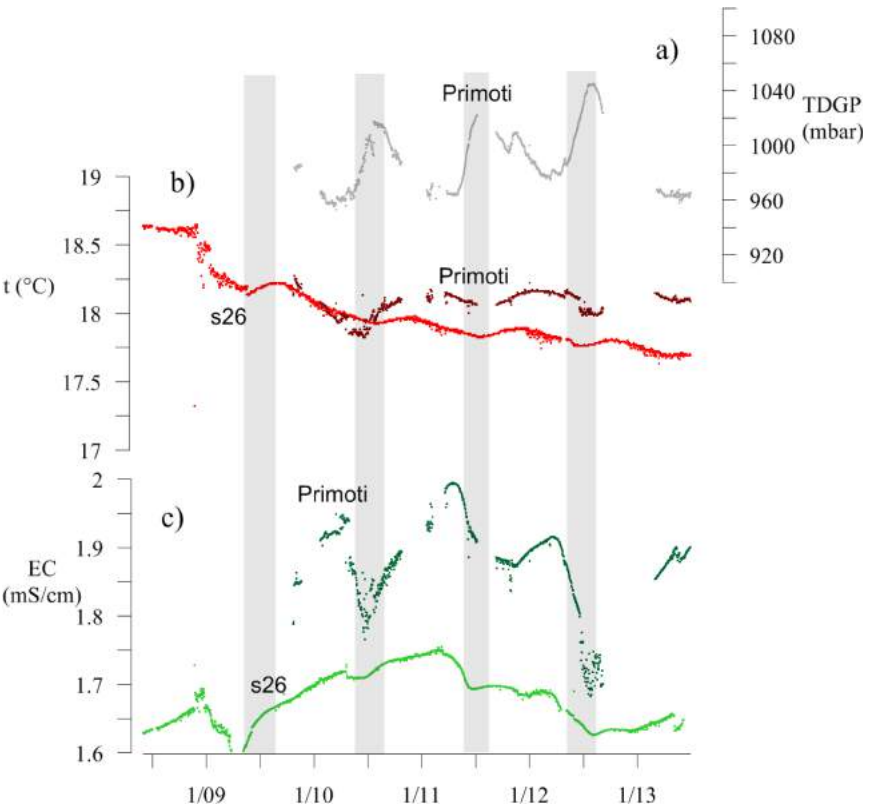

Figure 9. Time trends of (a) TDGP in Primoti well, (b) temperature, and (c) electrical conductivity (EC) recorded in the period between 2009 and 2013 in both Primoti well and s26 drainage gallery, in Zafferana-S. Venerina area. Shaded gray areas indicate the period April–July of every year.

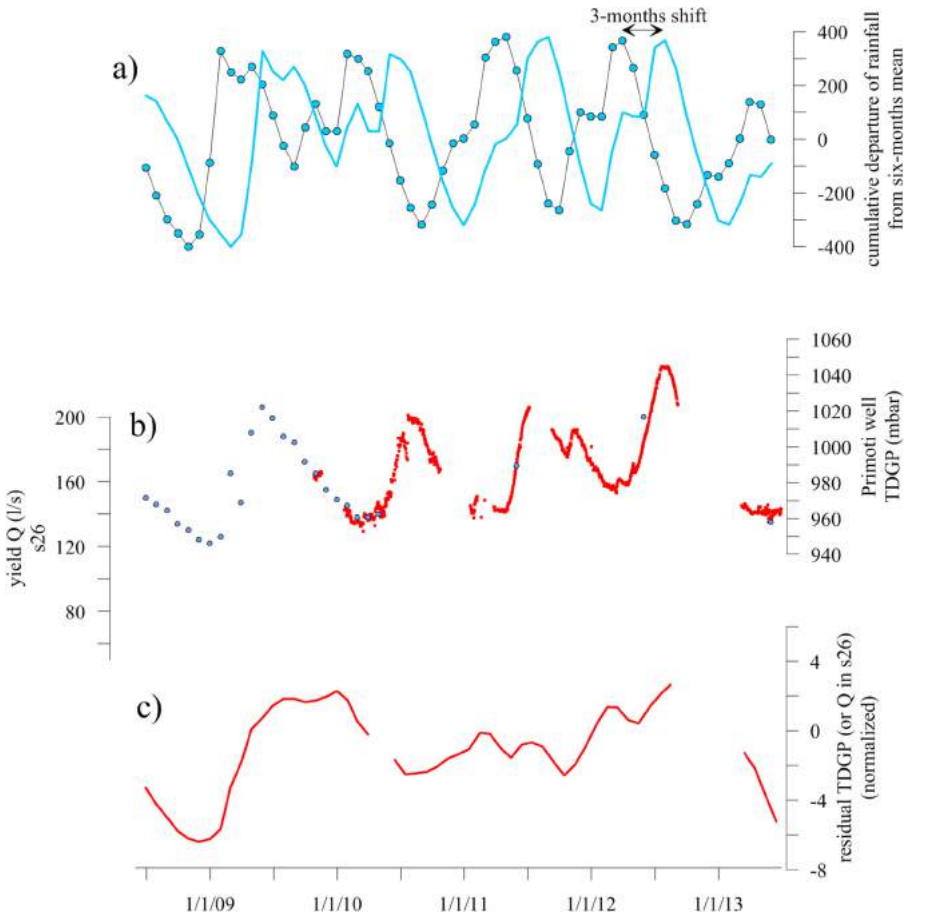

Figure 10. From the top to bottom: (a) the cumulative difference of monthly rainfall (www.osservatorioacque.it) with respect to the average of the previous 6 months (dotted line), and the same data delayed by 3 months (continuous line); (b) the yield values measured in the drainage gallery s26 (blue dots) and the TDGP (red dots) recorded in Primoti well; (c) the residual yield and TDGP (normalized by ensuring that values were always >0 by adding an arbitrary integer value to both series)), corrected for the effect of the rainfall amount.

particular, periods with increasing trends of EC values were observed during the year 2008 and from mid-2009 to early 2011, indicating the prevailing contribution of a more saline water end-member, peaking in late 2008. Conversely, decreases in EC values were observed both as short-term events, such as in early 2009, April 2010, March–June 2011 and March 2012, and as long-term events, such as from June 2011 to late 2012, all indicating a prevailing contribution of a less saline water end-member. The significant variations occurring in early 2009 and in 2012 can only be partially ascribed to changes in rainfall amount, given that the observed variations are much larger than those expected from a meteorological origin. Grey shaded areas in Figure 9 highlight the April–July period of every year, when the decrease of salinity may result from the delayed meteoric infiltration of rainfall and melted snow. The decrease of salinity is matched by a slight increase (as high as 60 mbar) of dissolved gas pressure (TDGP), which in this case may likely be considered a proxy for water table head. To apportion the effect of variable rainfall on the aquifer, we compared the data of yield, measured with monthly frequency in the drainage gallery s26, and TDGP (daily datum extracted from the hourly record in Primoti well) with the rainfall data provided by the meteorological network operating in Sicily (www.osservatorioacque.it). According to hydrological studies, water table heads and spring yields are generally correlated with the cumulative difference of monthly rainfall amount with respect to the average of the previous period [*Butterworth et al.,* 1999]. Figure 10a illustrates the cumulative difference of monthly rainfall (measured in the eastern flank, www.osservatorioacque.it) with respect to the average of the previous 6 months. Significant variations were recorded in the rainfall during the studied period. These variations clearly affect, with a delay of 3–5 months, both the yield of the drainage gallery s26 and the TDGP of well Primoti (Figure 10b), although this relationship does not always appears binding at a closer look. To apportion the effect of rainfall on the variations of yield and TDGP, we compared the

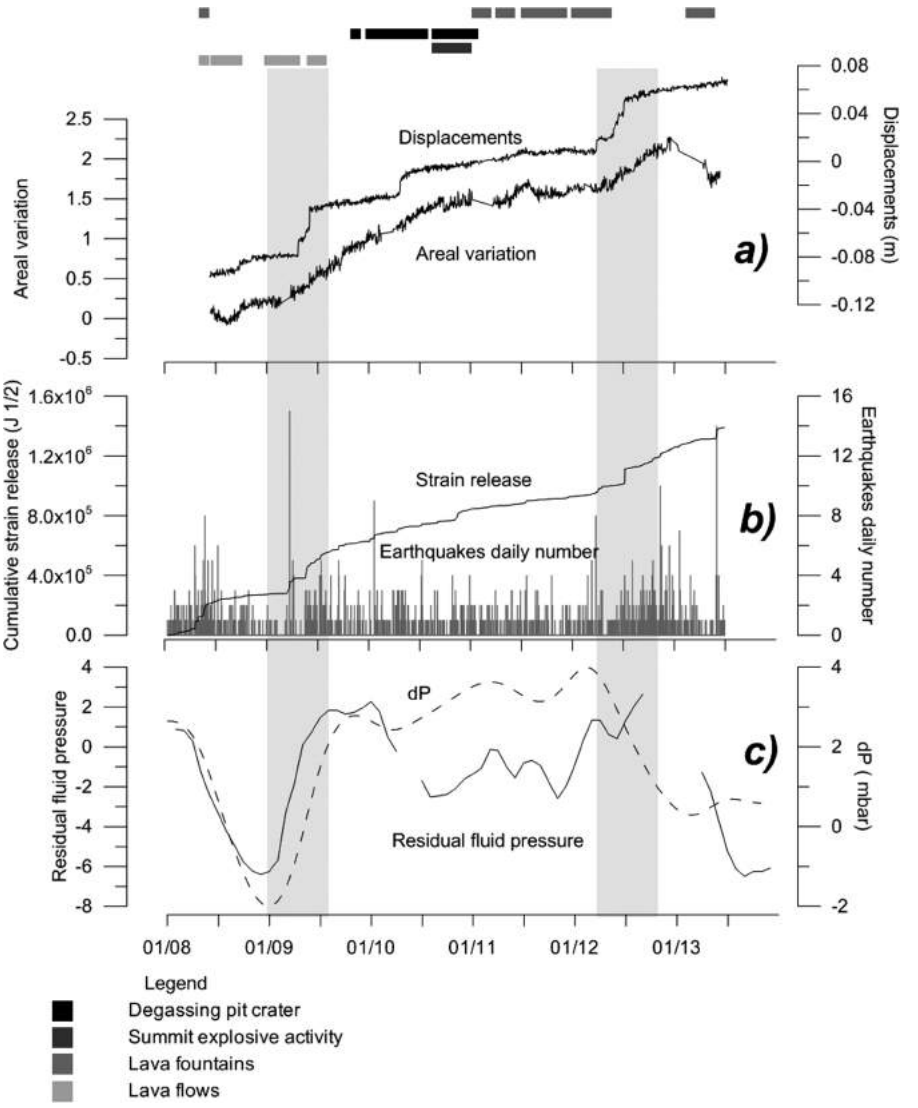

Figure 11. (a) Displacements recorded at Lachea station located on the lower East flank and the areal variation recorded by the stations EMAL-EMGL-EPLU on the upper Eastern flank. (b) Earthquakes daily number and cumulative strain release. (c) Temporal variation of fluid pressure, averaged over a 1 km-wide sector close to S. Venerina village (dP) and the normalized value of yield and water table head, assumed as a proxy for fluid pressure, recorded in s26 drainage gallery and in Primoti well, respectively, and corrected for the effect of rainfall (residual fluid pressure). The gray shaded area indicates two periods of coeval variations in observables, described in the main text. The different kinds of volcanic activity observed during the study period are represented in the top part of the plot.

cumulative sequences of their normalized values: to correct for the effect of rainfall, we subtracted the cumulative series of rainfall from the cumulative series of yield and TDGP, respectively (by considering a 3 month shift between the two signals). The corrected series is plotted in Figure 10c, which represents the residual yield and TDGP definitely, unrelated to the variations in the rainfall amount. Two major phases of decreasing TDGP and yield signals (both related to a fluid pressure drop) are shown in figure 10: the former in 2008 followed by a marked pressure increase in early 2009; the latter was observed as being steady in 2013. These variations were paralleled by changes in water salinity, as evidenced in figure 9.

4. Discussion

4.1. The General Framework: Comparing GPS, Seismic, and Geochemistry Data

The wealth of data described so far allow us to formulate a comprehensive interpretative model of the eastern flank dynamics in recent years. The most salient outcomes of our multiparametric analysis are summarized in the time plot of Figure 11. One of the most striking features of this analysis is the substantial

independence of observations from volcanic activity occurring during the study period (alternating phases of lava flows, lava fountains, and passive degassing). Nonetheless, the time changes of most parameters seem mutually and coherently related, thus suggesting a common cause. As described in the previous sections, the spring of 2009 marks a significant change in almost all the considered parameters. From April 2009 (Figure 11), the CGPS time series (a), and the strain release and number of VT earthquakes (b) changed their trends almost concurrently. In particular, this latter change consisted of an increase of both number and strain release of the VTs located in the eastern flank of Mt. Etna (see Figures 4 and 5). Moreover, during April–June 2009, also the LP event amplitudes showed the most significant increase, not temporally related to any eruptive activity (Figure 6f). Although some changes observed in our data during the considered period are occasionally not directly related to eruptive events, they are contemporary with the increase of CO_2 emissions from the lower eastern flank of the volcano, unrelated to the volcanic activity at the summit craters (Figure 8). These features are interpreted in terms of changes of fluid pressure within the volcanic system. Therefore, we believe that pressure changes beneath Etna's eastern flank could be responsible, among other causes, for its seaward movement. Indeed, fluid circulation can play a major role in the instability of volcanic edifices, and its effect is twofold. First, thermal fluids usually circulating in volcanic edifices drive an intense rock alteration and the precipitation of secondary minerals that weaken the physical characteristics of the rocks. Second, the increasing fluid pressure lowers the failure threshold, according to the modified Coulomb-Navier's failure criterion [e.g., *Stacey and Davis*, 2008].

Extensive fluid circulation beneath the eastern flank of Mt. Etna is well documented. The presence of gases or supercritical fluids in the eastern flank has been indicated by low Qp and low Vp anomalies, which are interpreted as an effect of a high pore pressure and intense faulting at depth of 0–6 km (Figure 7). Also, the most earthquakes on the eastern flank are recorded in this range of depth, probably an effect of fluid-induced rock failure, as observed worldwide in both volcanic and tectonic settings [e.g., *Christiansen et al*., 2005; *Ventura and Vilardo*, 2005; *Gudmundsson et al*., 2001].

As afore mentioned, the most important increase in LP amplitude occurred in April–June 2009, not during an eruptive period. Although this increase was in temporal agreement with the first SSE, during the second most important SSE (mid-2012) no amplitude increase was evident. Since most LP sources are located below the central craters [BN and VOR; e.g., *Cannata et al*., 2009], the difference in the behavior of the LPs recorded during the two afore mentioned SSEs is likely due to the distinct conditions of the shallow plumbing system feeding BN and VOR. Indeed, during 2009 the BN crater can be considered plugged, and hence an increase in the gas arrival can generate overpressure in the shallow feeding system, thus leading to an increase in the LP amplitude. On the other hand, in the second half of 2009, as well as in the summer of 2011 and 2012, explosive activity affected BN, modifying the conditions of the shallow part of the plumbing system. In particular, in June–July 2012 (right after the second SSE) strombolian activity occurred at BN, highlighting the arrival of fluids in the upper part of the BN plumbing system. In 2012 the different "unplugged" conditions did not allow the overpressure increase inside the plumbing system and thus the LP amplitude increase.

The presence of pressurized fluids in the eastern flank of the volcano, as deduced by seismic signals, is confirmed by the significant soil CO_2 degassing [*Giammanco and Bonfanti*, 2009, and references cited therein], as well as by the amount of dissolved CO_2 in groundwater, whose concentration is above the average for Etna's aquifers [*Brusca et al*., 2001]. Furthermore, a magnetotelluric study has also revealed the existence of hydrothermal fluids down to about 2 km of depth [*Siniscalchi et al*., 2012], within the clayey sedimentary basement where, owing to the low permeability of clays, fluid overpressure cannot readily hardly dissipate [*Reid*, 2004]. On these grounds, we can expect that the kinematics of the eastern flank can be triggered by a periodic increase of fluid pressure, particularly from the surface down to 3 km depth. One of these episodes likely occurred in April 2009, when a marked displacement was recorded in some GPS stations on the lower eastern flank. This episode closely follows the increase of areal dilatation (e.g., inflation) recorded at a few GPS stations in the summit area simultaneously with the increase of soil CO_2 degassing in the lower Eastern flank. These findings would poin to a fluid pressure increase in early 2009 in the volcano feeding system, which would have promoted both the CO_2 degassing and the acceleration of the lower eastern flank in April 2009. The coeval seismicity is probably fostered by the increased fluid circulation in this sector of the volcano. As shown in Figure 11, a similar pattern is observed in 2012, in a period of intense volcanic activity at the summit craters. In 2012, the inflation of the central part of the volcano is almost simultaneous with the spreading of the lower Eastern flank (Figure 12a) and to the increase of seismic release (Figure 11b). The

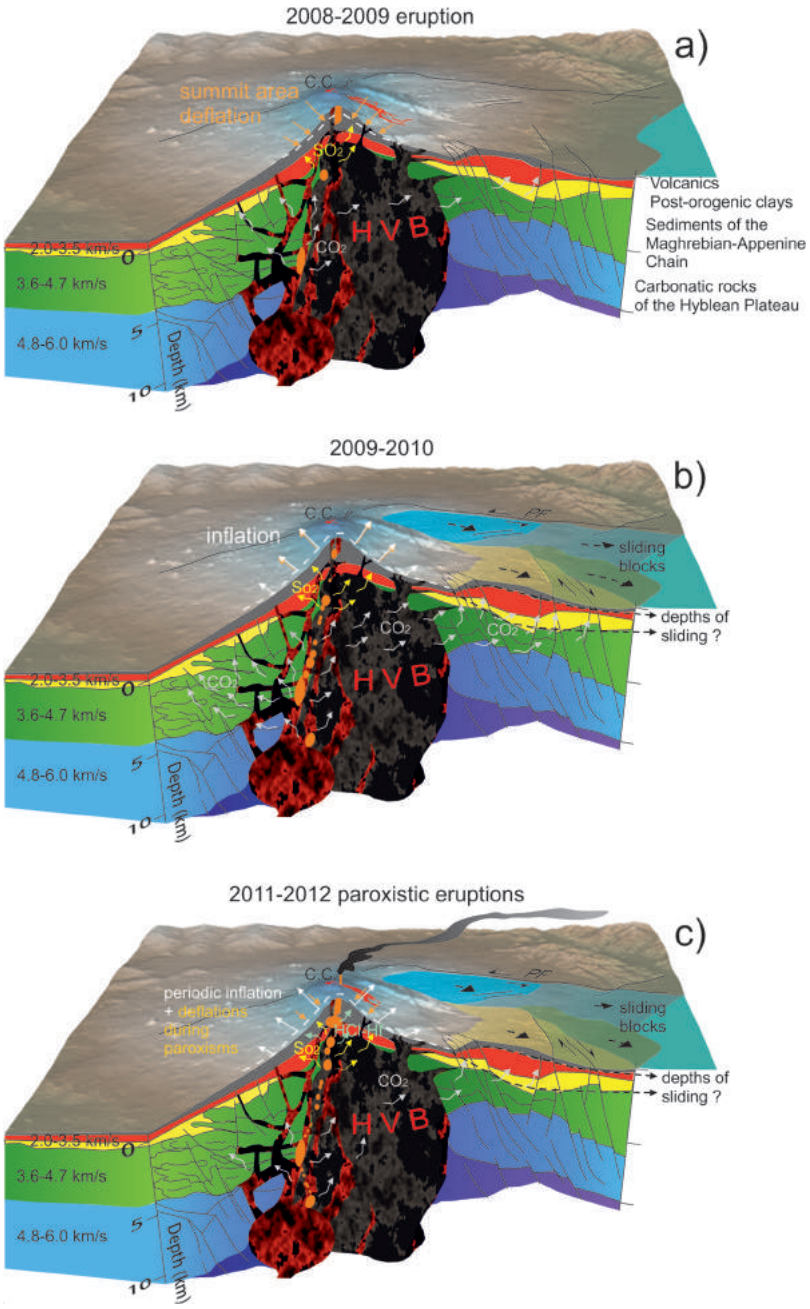

Figure 12. 3-D sketch of the model proposed in this work: (a) after the end of 2008 eruption a deflation took place. In this plot, the source of ground deformation as described in *Aloisi et al*. [2011a] is reported. This deflation induces a decompression in the upper levels of the volcano able to trigger a sudden (b) rising of magmatic fluids and the onset of an inflation (sources from *Aloisi et al*. [2011a]). These fluids trigger the large deformations observed through CGPS data (SSE). (c) This inflation anticipates the periods of lava fountains during 2011 and 2012 (see Figure 11). During the volcanic activity of 2011–2012, the displacements velocities decrease.

temporal pattern of soil CO_2 fluxes, as well as SO_2 and halogens (Figure 8), since early 2011, indicate that they are chiefly controlled by the degassing associated to the summit explosive activity. Nevertheless, during spring 2012, soil CO_2 fluxes show a temporary increase, diminishing at the end of the year, which could be ascribed, along with the inflation of the central part of the volcano, to an increase of the pressure of magmatic fluids. The two significant periods, highlighted in Figure 11, are matched by coeval compositional changes in groundwater in the Eastern flank (Figure 9). Fluid overpressure can be invoked as a mechanism for flank instability; analogously, deformation and fault movement can control fluid circulation. *Newhall et al*. [2001] describe various case studies concerning the effects of volcanic activity on the flow rate of

water from springs and wells. Changes in water circulation (observed as variations of spring outflow or piezometric level in wells) are interpreted as an effect of changes in crustal strain related to volcanic activity or to earthquakes [*Shibata and Akita*, 2001; *Hurwitz and Johnston*, 2003; *Koizumi et al*., 2004]. According to equation (1), fluid overpressure induces microfracturing [*Rojstaczer et al*., 2008; *Capasso et al*., 2014; *Claesson et al*., 2004], whereas the subsequent pressure drop and increase of permeability can locally modify fluid circulation, as foreseen by Darcy's Law [e.g., *Whitaker*, 1986].

Hydrofracturing is particularly efficient in the case of poorly permeable terrains (permeability lower than 10^{-13} m^2) [*Reid*, 2004]; otherwise, overpressure can dissipate by water outflow in springs, drainage galleries and streams, according to Darcy's Law. *Roeloffs and Linde* [2006] proposed the following relationship between the variation of volumetric crustal strain and that of fluid pressure (in the absence of fluid flow), which also includes variations due to changes in the mass of fluid per unit volume:

$$\Delta p = -(BK_u)\Delta\varepsilon_{kk} + \left[\frac{1}{1-K/K_S}\frac{m-m_0}{\rho_0}\right] \quad (1)$$

where B is a dimensionless material property (the Skempton's coefficient), K_u is the porous material's undrained bulk modulus, $\Delta\varepsilon_{kk}$ is the change in volumetric strain, K is the (drained) bulk modulus of the material, K_s is the bulk modulus of solid grains, $\frac{m-m_0}{\rho_0}$ is the change in fluid mass per unit of volume, divided by the fluid density in a reference state ρ_0. Variations of fluid pressure produced by changes of volumetric strain, according to equation (1), can be directly recorded as changes of water level in wells. The differential change of volumetric strain can thus induce spatial variation of the fluid pressure gradients and, as a consequence, a change in fluid circulation and discharge rates, according to the Darcy's law.

4.2. Crustal Strain and Groundwater Geochemistry Data: Evidence of Common Features

To verify the effects of the geodetic strain on fluid circulation, the GPS displacements were interpolated onto an equidistant grid (0.2 km grid spacing) by using two-dimensional splines [*Smith and Wessel*, 1990], and the geodetic 2-D strain tensor was calculated by the using the algorithm described in *Deniz and Ozener* [2010]. According to equation (1), and neglecting the change in fluid mass for the sake of simplicity, we modeled the areal distribution of the variation of fluid pressure related to the variation of the geodetic strain, retrieved from GPS data. The temporal variation of fluid pressure, averaged over a 1 km-wide sector close to S. Venerina village, are plotted in Figure 11c, together with the normalized value of yield and water table head, assumed as a proxy for fluid pressure, recorded in Primoti well and s26 drainage gallery and corrected for the effect of rainfall. The significant correlation between modeled and measured values strongly suggests that changes in fluid circulation in the eastern flank can be ascribed to changes in fluid pressure related to crustal strain. This affects also the physico-chemical characteristics of groundwater, as water transfer probably occurs among water bodies with different temperature and composition. Moreover, the ascent of CO_2-rich hydrothermal fluids can be either inhibited or enhanced, depending on the strain conditions, thus further modifying the composition of shallow aquifers. The change of fluid paths promoted by the changes of crustal strain likely causes the transfer of water in nearby basins and, as a consequence, a further variation of fluid pressure. This, in turn, can affect rock properties and ground movement, at least at shallow depth, where water circulation is more effective (i.e., at the volcanics-clays interface).

The whole data set suggests that shallow detachments located in the volcanic pile (upslope) or at its bottom (downslope), differentially involve distinct pre-existing blocks bounded by tectonic structures extending to deep crustal depth. To the north, the boundary is well constrained, being represented by the Pernicana fault that shows a tectonic origin only in its western sector. However, the lack of significant and well-defined deformation belts along the southern sliding boundary [*Azzaro et al*., 2013; *Branca et al*., 2014] and the occurrence of distinct blocks characterized by different motion interacting and rotating between each other [*Solaro et al*., 2010; *Bonforte et al*., 2011; *Bruno et al*., 2012] suggest that the process is much more complex and younger than is generally stated.

5. Conclusions: Toward a Synthetic Model to Explain the Large Displacements of Mt. Etna's Eastern Flank

The investigation into the possible sliding mechanisms of an entire sector of such a huge volcano as Mt. Etna, is in our opinion a thorny issue where the boundary between speculative aspects and objective

considerations is elusive. In this work, we analyze different data sets with the aim of finding some evidence that might define the simplest possible kinematic model. In our view the key factors that any model should consider are: (1) at Mt. Etna SSE events are clearly recognizable from GPS data; (2) their occurrence is not directly related to any significant seismic or volcanic event; (3) before these episodes, geochemical and geodetic (onset of an inflation, see Figure 11) data clearly show the arrival of fluids of volcanic origin; (4) increase in seismic strain release, related to VT earthquakes located in the volcano eastern flank, is coeval to two of these episodes; (5) water at the interface between the volcanic pile and the clays of Etna basement plays a major role and its circulation is linked to variations in the geodetically measured strain distribution. These data can be considered as the "variable part" of the model. Some other data, previously discussed, are the "fixed part" of the model, where the term "fixed" indicates the typical factors of the volcano itself and as the product of its geological history. These last factors are: (1) tomography of the volcano reveals that at least between 0 and 3 km b.s.l. pore pressure is very high and consequently fluids circulation is very effective; (2) GPS data reveal that displacements measured in the lower eastern flank of the volcano are greater than those measured in its upper part [*Bruno et al*., 2012] and that the variations in the time series of the station lying in the lower eastern flank are not identical; (3) InSAR data [e.g., *Solaro et al*., 2010] reveal that the eastern flank of Etna does not move as a single seaward sliding block, but rather it behaves as a group of clearly recognizable different blocks delimited by faults; this suggests that sliding processes must be framed within the morpho-structural setting of the volcanic edifice, since they involve pre-existing tectonic structures at shallow levels; (4) other geophysical data (electrical resistivity tomography, self-potential) in *Siniscalchi et al*. [2010] clearly indicate that there is an increased circulation of hydrothermal fluids in the NE sector of the volcano, able to induce instability. Magnetotelluric surveys [*Siniscalchi et al*., 2012] also confirm that several high-conductivity zones close to the main faults of the eastern flank suggest the presence of hydrothermal activity and fluid circulation that could enhance flank instability; (5) geological data collected along the shoreline of the eastern flank reveal that, in the last 20 ka, this part of the volcano has undergone uplift (up to 3 mm/yr) [*Branca et al*., 2014]. This process has locally and recently been interrupted by subsidence related to flank sliding of the volcanic edifice; (6) the recent (post-1970) magmatic activity of Mount Etna is characterized by a higher frequency of all types of eruption (including the subplinian ones) and higher effusion rates and by an increasing cumulative volume of the flank eruptions [*Schiano et al*., 2001; *Branca and Del Carlo*, 2004].

From this list of issues, the compelling argument is that any model to consider all these factors (and others) has to be both very simple in order to explain the first order characteristics related to the volcano considered as a geological subject, and complex enough in order to explain single episodes and transient behaviors observed in its history. With this two-fold objective in mind, we have tried to define a kinematic model that support both levels (Figure 12): The deflation of the volcanic edifice that accompanies the eruptive activity [e.g., *Bruno et al*., 2012] brings about a decompression that favors uprising of volatiles (Figure 12a). Hot magmatic fluids arrive from depth and ascend easily along the highly fractured eastern flank of Mt. Etna inducing both thermal and chemical mechanisms able to determine an alteration of the geotechnical characteristics of the lithotypes of Etna basement [e.g., *Mollo et al*., 2011; *Heap et al*., 2013]. These levels of altered rocks are detected by seismic and magnetotelluric tomography, also indicating a high pore pressure related to the multiple cracks induced by the alterations. The circulation of fluids is then facilitated in these cracks. The networks of cracks (Figure 12b), induced by the sudden arrival of fluids and by the action of other factors (gravity, unbuttressing of the eastern flank with respect to the others flanks, water circulation at the contact between the pile of lava and the clays of the basement), determine instability acting at different levels (depending essentially by the depth where the altered level is weaker). This could help to explain the presence of different blocks interacting and rotating between each other in the eastern flank [*Solaro et al*., 2010; *Bruno et al*., 2012].

Where the depth of the clayey levels is shallower, the dissipation of the movements is favored through creep mechanisms. These first two arguments can explain the main features of the kinematics observed in the eastern flank, but our data allow us to identify secondary factors (transients) that modify the ground deformation pattern of this sector of the volcano:

a. Strain patterns related to the action of volcanic sources influence the pore pressure of the shallower layers (mainly lava and pyroclastic deposits). Also these variations are able to induce movements particularly in the lower eastern flank, where the pile of volcanics is small. These variations of the strain acting on the flanks of the volcano can change the water circulation at the interface lava-basement.

b. Seismogenic reactivation of faults of the eastern flank can be dramatically influenced by the sudden upraise of dikes (e.g., 2002 eruption). These dikes can trigger earthquakes by Coulomb stress transfer between faults [*Bonanno et al*., 2011].

This model is corroborated by the data outlined in the previous chapters, but other considerations on a larger time scale can be made. The foremost concerns the large displacements observed in the eastern flanks from geodetic data or field observations. The contrast between the long term uplift of the area and the observed subsidence measured through geological data in the last 60 years and geodetic data in the last 25 years, can be reconciled only if we concede that this subsidence is not a permanent condition, but a transient phase, probably closely related to current volcanic activity. If the model proposed is valid, the large movements of the eastern flank are indeed a consequence of larger quantities of magmatic fluids circulating beneath it. As previously cited, since the second half of the past century [*Schiano et al*., 2001; *Branca and Del Carlo*, 2004] a growing number of all types of eruptions at Mt. Etna is well documented. The reasons for this increased activity are beyond the scope of this paper and, we confine our analysis to the simple evidence that, in our opinion, the two phenomena (larger displacements of the eastern flank and increasing number of eruptions) are the two sides of a single process.

Acknowledgments

The authors kindly acknowledge all those people involved in the difficult task of maintaining the complex monitoring system of Mt. Etna. The authors thank the 'INGV-CT Gruppo Analisi Dati Sismici' for their help in the analyses of the earthquakes. The original data used in this manuscript are available from these authors: M. Mattia for geodetic data (mario.mattia@ingv.it); A. Cannata for seismic data (andrea.cannata@ingv.it); W. D'Alessandro for groundwater data (walter.dalessandro@ingv.it); G. Salerno for SO2 flux data (giuseppe.salerno@ingv.it); S. Giammanco for CO_2 flux data [ZAF06] (salvatore.giammanco@ingv.it); M. Liuzzo for CO_2 flux data [p78] (marco.liuzzo@ingv.it) and Alessandro La Spina for HF/HCl data (alessandro.laspina@ingv.it). The AE Cin-Ty Lee and the anonymous reviewers provided us many useful suggestions that improved our manuscript.

References

A.A.V.V. (1979), *Carta geologica del Monte Etna. Scala 1: 50.000*, R. Romano Ed., L.A.C., Firenze.

Acocella, V., G. Puglisi, and F. Amelung (2013), Flank instability at Mt. Etna preface, *J. Volcanol. Geotherm. Res.*, *251*, 1–4.

Aloisi, M., M. Mattia, C. Ferlito, M. Palano, V. Bruno, and F. Cannavò (2011a), Imaging the multi-level magma reservoir at Mt. Etna volcano (Italy), *Geophys. Res. Lett.*, *38*, L16306, doi:10.1029/2011GL048488.

Aloisi, M., M. Mattia, C. Monaco, and F. Pulvirenti (2011b), Magma, faults, and gravitational loading at Mount Etna: The 2002–2003 eruptive period, *J. Geophys. Res.*, *116*, B05203, doi:10.1029/2010JB007909.

Alparone, S., G. Barberi, O. Cocina, E. Giampiccolo, C. Musumeci, and D. Patanè (2012), Intrusive mechanism of the 2008–2009 Mt. Etna eruption: Constraints by tomographic images and stress tensor analysis. *J. Volcanol. Geotherm. Res.*, *229*, 50–63.

Argnani, A., and C. Bonazzi (2005), Malta Escarpment fault zone offshore eastern Sicily: Pliocene-Quaternary tectonic evolution based on new multichannel seismic data, *Tectonics*, *24*, TC4009, doi:10.1029/2004TC001656.

Argnani, A., F. Mazzarini, C. Bonazzi, M. Bisson, and I. Isola (2013), The deformation offshore of Mount Etna as imaged by multichannel seismic reflection profiles, *J. Volcanol. Geotherm. Res.*, *251*, 50–64, doi:10.1016/j.jvolgeores.2012.04.016.

Azzaro, R. (1999), Earthquake surface faulting at Mount Etna volcano (Sicily) and implications for active tectonics, *J. Geodyn.*, *28*, 193–213.

Azzaro, R., M. S. Barbano, B. Antichi, and R. Rigano (2000), Macroseismic catalogue of Mt. Etna earthquakes from 1832 to 1998, *Acta Vulcanol.*, *12*, 3–36.

Azzaro, R., M. Mattia, and G. Puglisi (2001), Fault creep and kinematics of the eastern segment of the Pernicana fault (Mt. Etna, Sicily) derived from geodetic observations and their tectonic significance, *Tectonophysics*, *333*, 401–415.

Azzaro, R., A. Bonforte, S. Branca, and F. Guglielmino (2013), Geometry and kinematics of the fault systems controlling the unstable flank of Etna volcano (Sicily), *J. Volcanol. Geotherm. Res.*, *251*, 5–15.

Battaglia, M., C. Troise, F. Obrizzo, F. Pingue, and G. De Natale (2006), Evidence for fluid migration as the source of deformation at Campi Flegrei caldera (Italy), *Geophys. Res. Lett.*, *33*, L01307, doi:10.1029/2005GL024904.

Bonanno, A., M. Palano, E. Privitera, S. Gresta, and G. Puglisi (2011), Magma intrusion mechanisms and redistribution of seismogenic stress at Mt. Etna volcano (1997–1998), *Terra Nova*, *23*, 339–348, doi:10.1111/j.1365–3121.2011.01019.x.

Bonforte, A., and G. Puglisi (2003), Magma uprising and flank dynamics on Mount Etna volcano, studied using GPS data (1994–1995), *J. Geophys. Res.*, *108*(B3), 2153, doi:10.1029/2002JB001845.

Bonforte, A., and G. Puglisi (2006), Dynamics of the eastern flank of Mount Etna volcano (Italy) investigated by a dense GPS network, *J. Volcanol. Geotherm. Res.*, *153*, 357–369, doi:10.1016/j.jvolgeores.2005.12.005.

Bonforte, A., F. Guglielmino, M. Coltelli, A. Ferretti, and G. Puglisi (2011), Structural assessment of Mount Etna volcano from permanent scatterers analysis, *Geochem. Geophys. Geosyst.*, *12*, Q02002, doi:10.1029/2010GC003213.

Borgia, A., L. Ferrari, and G. Pasquarè (1992), Importance of gravitational spreading in the tectonic and volcanic evolution of Mount Etna, *Nature*, *357*, 231–235.

Branca, S., and P. Del Carlo (2004), *Eruptions of Mt. Etna during the past 3,200 years: A revised compilation integrating the historical and stratigraphic records, Mt. Etna: Volcano Laboratory*, edited by A. Bonaccorso, pp. 1–27, AGU, Washington, D. C., doi:10.1029/143GM02.

Branca, S., M. Coltelli, G. Groppelli, and F. Lentini (2011), Geological map of Etna volcano, 1:50,000 scale, *Ital. J. Geosci.*, *130*(3), 265–291, doi: 10.3301/IJG.2011.15.

Branca, S., G. De Guidi, G. Lanzafame, and C. Monaco (2014), Holocene vertical deformation along the coastal sector of Mt. Etna volcano (eastern Sicily, Italy): Implications on the time-space constrains of the volcano lateral sliding, *J. Geodyn.*, *82*, 194–203.

Brooks, B. A., J. H. Foster, M. Bevis, L. N. Frazer, C. J. Wolfe, and M. Behn (2006), Periodic slow earthquakes on the flank of Kilauea Volcano, Hawai'i, *Earth Planet. Sci. Lett.*, *246* (3/4), 207–216, doi:10.1016/j.epsl.2006.03.035.

Bruno, N., T. Caltabiano, S. Giammanco, and R. Romano (2001), Degassing of SO_2 and CO_2 at Mount Etna (Sicily) as an indicator of pre-eruptive ascent and shallow emplacement of magma, *J. Volcanol. Geotherm. Res.*, *110*, 137–153.

Bruno, V., M. Mattia, M. Aloisi, M. Palano, F. Cannavò, and W. E. Holt (2012), Ground deformations and volcanic processes as imaged by CGPS data at Mt. Etna (Italy) between 2003 and 2008, *J. Geophys. Res.*, *117*, B07208, doi:10.1029/2011JB009114.

Brusca, L., A. Aiuppa, W. D'Alessandro, F. Parello, P. Allard, and A. Michel (2001), Geochemical mapping of magmatic gaswater-rock interactions in the aquifer of Mount Etna volcano, *J. Volcanol. Geotherm. Res.*, *108*, 201–220.

Butterworth, J. A., R. E. Schulze, L. P. Simmonds, P. Moriarty, and F. Mugabe (1999), Hydrological processes and water resources management in a dryland environment IV: Long-term groundwater level fluctuations due to variation in rainfall, *Hydrol. Earth Syst. Sci.*, *3*, 353–361, doi:10.5194/hess-3-353-1999.

Calvari, S., G. G. Salerno, L. Spampinato, M. Gouhier, A. La Spina, E. Pecora, A. Harris, P. Labazuy, E. Biale, and E. Boschi (2011), An unloading foam model to constrain Etna's 11–13 January 2011 lava fountaining episode, *J. Geophys. Res.*, *116*, B11207, doi:10.1029/2011JB008407.
Campion, R., G. G. Salerno, P. F. Coheur, D. Hurtmans, L. Clarisse, K. Kazahaya, M. Burton, T. Caltabiano, C. Clerbaux, and A. Bernard (2010), Measuring volcanic degassing of SO_2 in the lower troposphere with ASTER band ratios, *J. Volcanol. Geotherm. Res.*, *194*, 1–3, 42–54.
Cannata, A., M. Hellweg, G. Di Grazia, S. Ford, S. Alparone, S. Gresta, P. Montalto, and D. Patanè (2009), Long period and very long period events at Mt. Etna volcano: Characteristics, variability and causality, and implications for their sources, *J. Volcanol. Geotherm. Res.*, *187*, 227–249, doi:10.1016/j.jvolgeores.2009.09.007.
Cannata, A., G. Di Grazia, M. Aliotta, C. Cassisi, P. Montalto, and D. Patanè (2013), Monitoring seismo-volcanic and infrasonic signals at volcanoes: Mt. Etna case study, *Pure Appl. Geophys.*, *170*, 1751–1771.
Capasso, G., C. Federico, P. Madonia, and A. Paonita (2014), Response of the shallow aquifer of the volcano-hydrothermal system during the recent crises at Vulcano Island (Aeolian Archipelago, Italy), *J. Volcanol. Geotherm. Res.*, *273*, 70–80, doi:10.1016/j.jvolgeores.2014.01.005.
Carroll, M. R., and J. R. Holloway (1994), Volatiles in magmas, *Rev. Mineral.*, *30*, 517.
Cervelli, P., P. Segall, K. Johnson, M. Lisowski, and A. Miklius (2002), Sudden aseismic fault slip on the south flank of Kilauea Volcano, *Nature*, *415*(6875), 1014–1018.
Chiocci, L. F., M. Coltelli, A. Bosman, and D. Cavallaro (2011), Continental margin large-scale instability controlling the flank sliding of Etna volcano, *Earth Planet. Sci. Lett.*, *305*, 57–64.
Chiodini, G., R. Cioni, M. Guidi, B. Raco, and L. Marini (1998), Soil CO_2 efflux measurements in volcanic and geothermal areas, *Appl. Geochem.*, *13*, 543–552.
Christiansen, L. B., S. Hurwitz, M. O. Saar, S. E. Ingebritsen, and P. A. Hsieh (2005), Seasonal seismicity at western United States volcanic centers, *Earth Planet. Sci. Lett.*, *240*, 307–321.
Cianetti S., C. Giunchi, and E. Casarotti (2012), Volcanic deformation and flank instability due to magmatic sources and frictional rheology: The case of Mount Etna, *Geophys. J. Int.*, *191*(3), 939–953, doi:10.1111/j.1365-246X.2012.05689.x.
Claesson, L., A. Skelton, C. Grahmn, C. Dietl, M. Mörth, P. Torssander, and I. Kockum (2004), Hydrogeochemical changes before and after a major earthquake, *Geololgy*, *32*(8), 641–644.
Cocina, O., G. Neri, E. Privitera, and S. Spampinato (1997), Stress tensor computations in the Mount Etna area (Southern Italy) and tectonic implications, *J. Geodyn.*, *23*, 109–127.
Continisio, R., F. Ferrucci, G. Gaudiosi, D. Lo Bascio, and G. Ventura (1997), Malta escarpment and Mt. Etna: Early stages of an asymmetric rifting process? Evidences from geophysical and geological data, *Acta Vulcanol.*, *9*, 45–53.
Corsaro, R. A., and R. Cristofolini (2000), Subaqueous volcanism in the Etnean area: Evidence for hydromagmatic activity and regional uplift inferred from the Castle Rock of Acicastello, *J. Volcanol. Geotherm. Res.*, *95*, 209–225.
Corsaro, R. A., M. Neri, and M. Pompilio (2002), Paleo-environmental and volcano-tectonic evolution of the south-eastern flank of Mt. Etna during the last 225 ka inferred from volcanic succession of the "Timpe", Acireale, Sicily, *J. Volcanol. Geotherm. Res.*, *113*, 289–306.
Davis, D., J. Suppe, and F.A. Dahlen (1993), Mechanics of fold-and-thrust belts and accretionary wedges, *J. Geophys. Res.*, *88*, 1153–1172.
Day, S. J. (1996), Hydrothermal pore fluid pressure and the stability of porous, permeable volcanoes, *Geol. Soc. Spec. Publ.*, *110*(1), 77–93.
De Gregorio, S., S. Gurrieri, and M. Valenza (2005), A PTFE membrane for the in situ extraction of dissolved gases in natural waters: Theory and applications, *Geochem. Geophys. Geosyst.*, *6*, Q09005, doi:10.1029/2005GC000947.
De Guidi, G., G. Barberi, G. Barreca, V. Bruno, F. Cultrera, S. Grassi, S. Imposa, M. Mattia, L. Scarfì, and S. Scudero (2013), Geological, seismological and geodetic evidence of active thrusting and folding south of Mt. Etna (eastern Sicily), Atti 32° Convegno Nazionale G.N.G.T.S., Trieste 19–21 Novembre 2013, Tema 1: Geodinamica, 48–53.
Deniz, I., and H. Ozener (2010), Estimation of strain accumulation of densification network in Northern Marmara Region, Turkey, *Nat. Hazards Earth Syst. Sci.*, *10*(10), 2135–2143.
Di Grazia, G., S. Falsaperla, and H. Langer (2006), Volcanic tremor location during the 2004 Mount Etna lava effusion, *Geophys. Res. Lett.*, *33*, L04304, doi:10.1029/2005GL025177.
Dragert, H., K. Wang, and G. Rogers (2004), Geodetic and seismic signatures of episodic tremor and slip in the northern Cascadia subduction zone, *Earth Planets Space*, *56*(12), 1143–1150.
Dzurisin, D., C. Wicks, and W. Thatcher (1999), Renewed uplift at the Yellowstone caldera measured by leveling surveys and satellite radar interferometry, *Bull. Vulcanol.*, *61*, 349–355.
Firth, C., I. Stewart, W. J. McGuire, S. Kershaw, and C. Vita-Finzi (1996), Coastal elevation changes in eastern Sicily: Implications for volcano instability at Mount Etna, *Geol. Soc. Spec. Publ.*, *110*(1), 153–167.
Froger, J. L., O. Merle, and P. Briole (2001), Active spreading and regional extension at Mount Etna imaged by SAR interferometry, *Earth Planet. Sci. Lett.*, *148*, 245–258.
Giammanco, S., and P. Bonfanti (2009), Cluster analysis of soil CO_2 data from Mt. Etna (Italy) reveals volcanic influences on temporal and spatial patterns of degassing, *Bull. Volcanol.*, *71*, 201–218, doi:10.1007/s00445-008-0218-x.
Giammanco, S., S. Gurrieri, and M. Valenza (1995), Soil CO_2 degassing on Mt. Etna (Sicily) during the period 1989–1993: Discrimination between climatic and volcanic influences, *Bull. Volcanol.*, *57*, 52–60.
Giammanco, S., S. Inguaggiato, and M. Valenza (1998), Soil and fumarole gases of Mount Etna: Geochemistry and relations with volcanic activity, *J. Volcanol. Geotherm. Res.*, *81*, 297–310.
Gillot, P. Y., G. Kieffer, and R. Romano (1994), The evolution of Mount Etna in the light of potassium-argon dating, *Acta Vulcanol.*, *5*, 81–87.
Gottsmann, J., R. Carniel, N. Coppo, L. Wooller, S. Hautmann, and H. Rymer (2007), Oscillations in hydrothermal systems as a source of periodic unrest at caldera volcanoes: Multiparameter insights from Nisyros, Greece, *Geophys. Res. Lett.*, *34*, L07307, doi:10.1029/2007GL029594.
Gresta, S., V. Longo, and A. Viavattene (1990), Geodynamic behaviour of eastern and western sides of Mount Etna, *Tectonophysics*, *179*, 81–92.
Gresta, S., D. Bella, C. Musumeci, and P. Carveni (1997), Some efforts on active faulting processes (earthquake and aseismic creep) acting on the eastern flank of Mt. Etna (Sicily), *Acta Vulcanol.*, *9*, 101–107.
Gresta, S., L. Peruzza, D. Slejko, and G. Distefano (1998), Inferences on the main volcano-tectonic structures at Mt. Etna (Sicily) from a probabilistic seismological approach, *J. Seismol.*, *2*, 105–116.
Gudmundsson, A., S. S. Berg, K. B. Lyslo, and E. Skurtveit (2001), Fracture networks and fluid transport in active fault zones, *J. Struct. Geol.*, *23*, 343–353.
Guest, J. E., D. K. Chester, and A. M. Duncan (1984), The Valle del Bove, Mount Etna: Its origin and relations to the stratigraphy and structure of the volcano, *J. Volcanol. Geotherm. Res.*, *21*, 1–23.
Gurrieri, S., and M. Valenza (1988), Gas transport in natural porous mediums: A method for measuring CO_2 flows from the ground in volcanic and geothermal areas, *Rend. Soc. Ital. Mineral. Petrol.*, *43*, 1151–1158.

Gurrieri, S., M. Liuzzo, and G. Giudice (2008), Continuous monitoring of soil CO_2 flux on Mt. Etna: The 2004–2005 eruption and the role of regional tectonics and volcano tectonics, *J. Geophys. Res.*, *113*, B09206, doi:10.1029/2007JB005003.
Heap M. J., S. Mollo, S. Vinciguerra, Y. Lavallée, K.-U. Hess, D. B. Dingwell, P. Baud, and G. Iezzi, 2013. Thermal weakening of the carbonate basement under Mt. Etna volcano (Italy): Implications for volcano instability, *J. Volcanol. Geotherm. Res.*, *250*, 42–60, doi:10.1016/j.jvolgeores.2012.10.004.
Herring, T. A. (2004), *GLOBK: Global Kalman Filter VLBI and GPS Analysis Program, Version 10.2, User's Manual*, MIT Press, Cambridge, U. K.
Hill, D. P., F. Pollitz, and C. Newhall (2002), Earthquake-volcano interactions, *Phys. Today*, *55*(11), 41–47.
Hirn, A., R. Nicolich, J. Gallart, M. Laigle, L. Cernobori, and ETNASEIS Scientific Group (1997), Roots of Etna volcano in faults of great earthquakes, *Earth Planet. Sci. Lett.*, *148*, 171–191.
Hurwitz, S., and M. J. S. Johnston (2003), Groundwater level changes in a deep well in response to a magma intrusion event on Kilauea Volcano, Hawai'i, *Geophys. Res. Lett.*, *30*(22), 2173, doi:10.1029/2003GL018676.
Kieffer, G. (1983), L'évolution structurale de l'Etna (Sicile) et les modalités du contrôle tectonique et volcano-tectonique de son activité. Faits et hypothèses après les éruptions de 1978 et 1979, *Rev. Géogr. Phys. Géol. Dyn.*, *24*(2), 89–100.
King, R. W., and Y. Bock (2004), *Documentation of the MIT GPS Analysis Software: GAMIT, Release 10.2, User's Manual*, MIT Press, Cambridge, U. K.
Koizumi, N., Y. Kitagawa, N. Matsumoto, M. Takahashi, T. Sato, O. Kamigaichi, and K. Nakamura (2004), Preseismic groundwater level changes induced by crustal deformations related to earthquake swarms off the east coast of Izu Peninsula, Japan, *Geophys. Res. Lett.*, *31*, L10606, doi:10.1029/2004GL019557.
Labaume, P., J. C. Bousquet, and G. Lanzafame (1990), Early deformations at a submarine compressive front: The Quaternary Catania foredeep south of Mt. Etna, Sicily, Italy, *Tectonophysics*, *177*, 349–366.
Lanzafame, G., M. Neri, and D. Rust (1996), Active tectonics affecting the eastern flank of Mount Etna: Structural interactions at regional and local scale, in Proceedings of the Conference on Etna, edited by P. H. Gravestock and W.J. McGuire, pp. 25–33.
Larson, K. M., A. R. Lowry, V. Kostoglodov, W. Hutton, O. Sanchez, K. Hudnut, and G. Suarez (2004), Crustal deformation measurements in Guerrero, Mexico, *J. Geophys. Res.*, *109*, B04409, doi:10.1029/2003JB002843.
La Spina, A., M. Burton, and G. Salerno (2010), Unravelling the processes controlling gas emissions from the central and northeast craters of Mt. Etna, *J. Volcanol. Geotherm. Res.*, *198*, 368–376, doi:10.1016/j.jvolgeores.2010.09.018.
Liuzzo, M., S. Gurrieri, G. Giudice, and G. Giuffrida (2013), Ten years of soil CO2 continuous monitoring on Mt. Etna: Exploring the relationship between processes of soil degassing and volcanic activity, *Geochem. Geophys. Geosyst.*, *14*, 2886–2899, doi:10.1002/ggge.20196.
Lo Giudice, E., and R. Rasà (1986), The role of the NNW structural trend in the recent geodynamic evolution of north-eastern Sicily and its volcanic implications in the Etnean area, *J. Geodyn.*, *25*, 309–330.
Lo Giudice, E., and R. Rasà (1992), Very shallow earthquakes and brittle deformation in active volcanic areas: The Etnean region as an example, *Tectonophysics*, *202*, 257–268.
Lo Giudice, E., G. Patanè, R. Rasà, and R. Romano (1982), The structural framework of Mount Etna, *Mem. Soc. Geol. Ital.*, *23*, 125–158.
Lundgren, P., P. Berardino, M. Coltelli, G. Fornaro, R. Lanari, G. Puglisi, E. Sansosti, and M. Tesauro (2003), Coupled magma chamber inflation and sector collapse slip observed with SAR interferometry on Mt. Etna volcano, *J. Geophys. Res.*, *108*(B5), 2247, doi:10.1029/2001JB000657.
Lundgren, P., F. Casu, M. Manzo, A. Pepe, P. Berardino, E. Sansosti, and R. Lanari (2004), Gravity and magma induced spreading of Mount Etna volcano revealed by satellite radar interferometry, *Geophys. Res. Lett.*, *31*, L04602, doi:10.1029/2003GL018736.
Mao, A., C.G.A. Harrison, and T. H. Dixon (1999), Noise in GPS coordinate time series, *J. Geophys. Res.*, *104*, 2797–2816, doi:10.1029/1998JB900033.
McGuire, W. J., and S. J. Saunders (1993), *Recent earth movements at active volcanoes: A review. Quat. Proc.*, *3*, 33–46.
Merucci, L., M. Burton, S. Corradini, and G. G. Salerno (2011), Reconstruction of SO_2 flux emission chronology from space-based measurements, *J. Volcanol. Geotherm. Res. 206*, 80–87.
Miyazaki, S., J. McGuire, and P. Segall (2003), A transient subduction zone slip episode in southwest Japan observed by the nationwide GPS array, *J. Geophys. Res.*, *108*(B2), 2087, doi:10.1029/2001JB000456.
Miyazaki, S., P. Segall, J. J. McGuire, and T. Kato (2006), Spatial and temporal evolution of stress and slip rate during the 2000 Tokai slow earthquake, *J. Geophys. Res.*, *111*, B03409, doi:10.1029/2004JB003426.
Mollo S., S. Vinciguerra, G. Iezzi, A. Iarocci, P. Scarlato, M. J. Heap, and D. B. Dingwell (2011), Volcanic edifice weakening via devolatilization reactions, *Geophys. J. Int.*, *186*, 1073–1077.
Monaco, C., L. Petronio, and M. Romanelli (1995), Tettonica estensionale nel settore orientale del Monte Etna (Sicilia): Dati morfotettonici e sismici, *Studi Geol. Camerti*, *2*, 363–374.
Monaco, C., P. Tapponnier, L. Tortorici, and P. Y. Gillot (1997), Late Quaternary slip rates on the Acireale-Piedimonte normal faults and tectonic origin of Mt. Etna (Sicily), *Earth Planet. Sci. Lett.*, *147*, 125–139.
Monaco, C., M. Bianca, S. Catalano, G. De Guidi, and L. Tortorici (2002), Sudden change in the Late Quaternary tectonic regime in eastern Sicily: Evidences from geological and geomorphological features, *Boll. Soc. Geol. Ital.*, *1*, 901–913.
Monaco C., S. Catalano, O. Cocina, G. De Guidi, C. Ferlito, S. Gresta, C. Musumeci, and L. Tortorici (2005), Tectonic control on the eruptive dynamics at Mt. Etna volcano (eastern Sicily) during the 2001 and 2002–2003 eruptions, *J. Volcanol. Geotherm. Res.*, *144*, 221–233.
Monaco, C., G. De Guidi, and C. Ferlito (2010), The morphotectonic map of Mt. Etna, *Ital. J. Geosci.*, *129*(3), 408–428.
Montgomery-Brown, E. K., P. Segall, and A. Miklius (2009), Kilauea slow slip events: Identification, source inversions, and relation to seismicity, *J. Geophys. Res.*, *114*, B00A03, doi:10.1029/2008JB006074.
Neri, M., V. Acocella, and B. Behncke (2004), The role of the Pernicana Fault System in the spreading of Mt. Etna (Italy) during the 2002–2003 eruption, *Bull. Volcanol.*, *66*, 417–430, doi:10.1007/s00445-003-0322-x.
Newhall, C. G., S. E. Albano, N. Matsumoto, and T. Sandoval (2001), Roles of groundwater in volcanic unrest, *J. Geol. Soc. Philipp.*, *56*, 69–84.
Nicolich, R., M. Laigle, A. Hirn, L. Cernobori, and J. Gallart (2000), Crustal structure of the Ionian margin of Sicily: Etna volcano in the frame of regional evolution, *Tectonophysics*, *329*, 121–139.
Palano, M., L. Ferranti, C. Monaco, M. Mattia, M. Aloisi, V. Bruno, F. Cannavò, and G. Siligato (2012), GPS velocity and strain fields in Sicily and southern Calabria, Italy: Updated geodetic constraints on tectonic block interaction in the central Mediterranean, *J. Geophys. Res.*, *117*, B07401, doi:10.1029/2012JB009254.
Pan, V., J. R. Holloway, and R. L. Hervig (1991), The pressure and temperature dependence of carbon dioxide solubility in tholeiitic basalt melts, *Geochim. Cosmochim. Acta*, *55*, 1587–1595.
Parkinson, K. J. (1981), An improved method for measuring soil respiration in the field, *J. Appl. Ecol.*, *18*, 221–228.
Patanè, D., and E. Privitera (2001), Seismicity related to 1989 and 1991-93 Mt. Etna (Italy) eruptions: Kinematic constraints by FPS analysis, *J. Volcanol. Geotherm. Res.*, *109*, 77–98.

Patanè, D., C. Chiarabba, O. Cocina, P. De Gori, M. Moretti, and E. Boschi (2002), Tomographic images and 3D earthquake locations of the seismic swarm preceding the 2001 Mt. Etna eruption: Evidence for a dyke intrusion, *Geophys. Res. Lett.*, *29*(10), 1497, doi:10.1029/2001GL014391.

Patanè, D., C. Chiarabba, P. De Gori, and A. Bonaccorso (2003), Magma ascent and the pressurization of Mt. Etna's volcanic system, *Science*, *299*, 2061–2063.

Patanè, D., O. Cocina, S. Falsaperla, E. Privitera, and S. Spampinato (2004), Mt. Etna volcano: A seismological framework, in *Mt. Etna: Volcano Laboratory, Geophys. Monogr. Ser.*, vol. 143, edited by A. Bonaccorso et al., pp. 147–165, AGU, Washington, D. C.

Patanè D., M. Mattia, and M. Aloisi (2005), Shallow intrusive processes during 2002–2004 and current volcanic activity on Mt. Etna, *Geophys. Res. Lett.*, *32*, L06302, doi:10.1029/2004GL021773.

Patanè, G., S. La Delfa, and J. C. Tanguy (2006), Volcanism and mantle-crust evolution: The Etna case, *Earth Planet. Sci. Lett.*, *241*, 831–843.

Patanè, D., et al. (2013), Insights into magma and fluid transfer at Mount Etna by a multiparametric approach: A model of the events leading to the 2011 eruptive cycle, *J. Geophys. Res. Solid Earth*, *118*, 3519–3539, doi:10.1002/jgrb.50248.

Puglisi, G., and A. Bonforte (2004), Dynamics of Mount Etna volcano inferred from static and kinematic GPS measurements, *J. Geophys. Res.*, *109*, B11404, doi:10.1029/2003JB002878.

Rasá, R., R. Azzaro, and O. Leonardi (1996), Aseismic creep on faults and flank instability at Mount Etna volcano, Sicily, *Geol. Soc. Spec. Publ.*, *110*(1), 179–192.

Reid, M. E. (2004), *Massive collapse of volcano edifices triggered by hydrothermal pressurization*, Geology, 32, 373–376.

Roeloffs, E. A., and A. T. Linde (2006), Borehole observations of continuous strain and fluid pressure, in *Volcano Deformation: Geodetic Monitoring Techniques*, edited by D. Dzurisin, chap. 9, pp. 305–322, Springer, Chichester, U. K.

Rojstaczer, S. A., S. E. Ingebritsen, and D. O. Hayba (2008), Permeability of continental crust influenced by internal and external forcing, *Geofluids*, *8*, 128–139.

Rust, D., and M. Neri (1996), The boundaries of large-scale collapse on the flanks of Mount Etna, Sicily, *Geo. Soc. Spec. Publ.*, *110*(1), 193–208.

Rust, D., B. Behncke, M. Neri, and A. Ciocanel (2005), Nested zone of instability in the Mount Etna volcanic edifice, Italy, *J. Volcanol. Geotherm. Res.*, *144*, 137–153.

Salerno, G. G., M. Burton, C. Oppenheimer, T. Caltabiano, D. Randazzo, and N. Bruno (2009a), Three-years of SO_2 flux measurements of Mt. Etna using an automated UV scanner array: Comparison with conventional traverses and uncertainties in flux retrieval, *J. Volcanol. Geotherm. Res.*, *183*, 76–83, doi:10.1016/j.jvolgeores.2009.02.013.

Salerno, G. G., M. R. Burton, C. Oppenheimer, T. Caltabiano, V. Tsanev, and N. Bruno (2009b), Novel retrieval of volcanic SO_2 abundance from ultraviolet spectra, *J. Volcanol. Geotherm. Res.*, *181*, 141–153, doi:10.1016/j.jvolgeores.2009.01.009.

Scarfì, L., A. Messina, and C. Cassisi (2013), Sicily and Southern Calabria focal mechanism database: A valuable tool for the local and regional stress field determination, *Ann. Geophys.*, *56*(1), D0109, doi:10.4401/ag-6109.

Schiano, P., R. Clocchiatti, L. Ottolini, and T. Busà (2001), Transition of Mount Etna lavas from a mantle-plume to an island-arc magmatic source, *Nature*, *412*(6850), 900–904.

Segall, P., E. K. Desmarais, D. Shelly, A. Miklius, and P. Cervelli (2006), Earthquakes triggered by silent slip events on Kīauea volcano, Hawaii, *Nature*, *442*(7098), 71–74.

Shibata, T., and F. Akita (2001), Precursory changes in well water level prior to the March, 2000 eruption of Usu volcano, Japan, *Geophys. Res. Lett.*, *28*, 1799–1802.

Siniscalchi, A., S. Tripaldi, M. Neri, S. Giammanco, S. Piscitelli, M. Balasco, B. Behncke, C. Magri, V. Naudet, and E. Rizzo (2010), Insights into fluid circulation across the Pernicana Fault (Mt. Etna, Italy) and implications for flank instability, *J. Volcanol. Geotherm. Res.*, *193*(1), 137–142.

Siniscalchi, A., S. Tripaldi, M. Neri, M. Balasco, G. Romano, J. Ruch, and D. Schiavone (2012), Flank instability structure of Mt. Etna inferred by a magnetotelluric survey, *J. Geophys. Res.*, *117*, B03216, doi:10.1029/2011JB008657.

Smith, W. H. F., and P. Wessel (1990), Gridding with continuous curvature splines in tension, *Geophysics*, *55*, 3 293–305.

Solaro, G., V. Acocella, S. Pepe, J. Ruch, M. Neri, and E. Sansosti (2010), Anatomy of an unstable volcano from InSAR: Multiple processes affecting flank instability at Mt. Etna, 1994–2008, *J. Geophys. Res.*, *115*, B10405, doi:10.1029/2009JB000820.

Stacey, F. D., and P. M. Davis (2008), *Physics of the Earth*, 4th ed., 532 pp., Cambridge Univ. Press, Cambridge, U. K.

Tanguy, J. C., and G. Kieffer (1993), Les eruption del'Etna et leurs mécanismes, *Mém. Soc. Géol. France*, *163*, 239–252.

Thomas, M. E., N. Petford, and E. N. Bromhead (2004), The effect of internal gas pressurization on volcanic edifice stability: Evolution towards a critical state, *Terra Nova*, *16*, 312–317.

Tibaldi, A., and G. Groppelli (2002), Volcano-tectonic activity along structures of the unstable NE flank of Mt. Etna (Italy) and their possible origin, *J. Volcanol. Geotherm. Res.*, *115*, 277–302.

Ventura, G. and G. Vilardo (2005), Estimates of fluid pressure and tectonic stress in hydrothermal/volcanic areas: A methodological approach, *Ann. Geophys.*, *48*(4–5), 797–803.

Voight, B., and D. Elsworth (2000), Instability and collapse of hazardous gas-pressurized lava domes, *Geophys. Res. Lett.*, *27*, 1–4.

Wezel, F. C. (1967), I terreni quaternari del substrato dell'Etna, *Atti Acc. Gioienia Sc. Nat. Catania*, *6*, 271–282.

Whitaker, S. (1986), Flow in porous media I: A theoretical derivation of Darcy's law, *Transp. Porous Media*, *1*, 3–25.

Wolfe, C. J., P. G. Okubo, and P. M. Shearer (2003), Mantle fault zone beneath Kilauea volcano, Hawaii, *Science*, *300*(5618), 478–480.

Erratum

In the originally published version of this article, the following reference should have been included:

Alparone, S., G. Barberi, O. Cocina, E. Giampiccolo, C. Musumeci, and D. Patanè (2012). Intrusive mechanism of the 2008–2009 Mt. Etna eruption: Constraints by tomographic images and stress tensor analysis, *J. Volcanol. Geotherm. Res.*, 229, 50–63.

The reference also should have been included in the following areas:

In section 3.2.1., "In particular, here we reanalyze the results obtained by the last tomographic study performed by *Patanè et al.* [2006] integrating them with other results and new unpublished data" should be "In particular, here we reanalyze the results obtained by the last tomographic study performed by *Patanè et al.* [2006] and *Alparone et al.* [2012]."

In the Figure 7 caption, "Tomographic image of Mt. Etna (modified from data previously published by *Patanè et al.* [2006] and integrated with new data)" should be "Tomographic image of Mt. Etna (modified from data previously published by *Patanè et al.* [2006] and *Alparone et al.* [2012])."